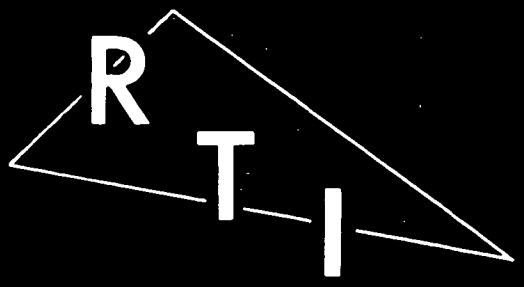

RESEARCH TRIANGLE INSTITUTE

NASA CR-111931-1

AN ANALYTICAL INVESTIGATION OF ACQUISITION TECHNIQUES AND SYSTEM INTEGRATION STUDIES FOR A RADAR AIRCRAFT GUIDANCE RESEARCH FACILITY

PHASE II - Final Report Supplement

By

W. S. Thompson and W. H. Ruedger
Research Triangle Institute

Langley Technical Representative:
R. F. Emond
Langley Research Center

Prepared Under Contract No. NAS1-8912
By
Research Triangle Institute

For

National Aeronautics and Space Administration

RTI No. 43U-443-1

April 1973

NASA CR-111931-1

AN ANALYTICAL INVESTIGATION OF ACQUISITION TECHNIQUES AND SYSTEM INTEGRATION STUDIES FOR A RADAR AIRCRAFT GUIDANCE RESEARCH FACILITY

PHASE II - Final Report Supplement

By

W. S. Thompson and W. H. Ruedger
Research Triangle Institute

Langley Technical Representative:
R. F. Emond
Langley Research Center

Prepared Under Contract No. NAS1-8912
By
Research Triangle Institute

For

National Aeronautics and Space Administration

RTI No. 43U-443-1

April 1973

TABLE OF CONTENTS

LIST OF ILLUSTRATIONS

LIST OF ILLUSTRATIONS, Continued

LIST OF TABLES

ABSTRACT

A review of NASA Langley Research Center (LRC) user requirements and updated instrumentation plans are presented for the aircraft tracking and guidance facility at NASA Wallops Station. User demand has increased as a result of new flight research programs; however, basic requirements remain the same as originally reported. Instrumentation plans remain essentially the same but with plans for up- and down-link telemetry more firm. With slippages in the laser acquisition schedule, added importance is placed on the FPS-16 radar as the primary tracking device until the laser is available.

Limited simulation studies of a particular Kalman-type filter are also presented herein. These studies simulated the use of the filter in a helicopter guidance loop in a real-time mode. Disadvantages and limitations of this mode of operation are pointed out.

Laser eyesafety calculations show that laser tracking of aircraft is readily feasible from the eyesafety viewpoint.

SUMMARY AND RECOMMENDATIONS

This report is a supplement to an earlier report (ref. 1) submitted on a study of requirements and instrumentation for improvements to the NASA Wallops runway facility. Basic requirements and plans for the facility have remained essentially the same over the past year, and except for slippage in the original laser procurement, acquisition of the improved facility is proceeding on schedule. Installation of the FPS-16 radar has been completed, and following the delivery, checkout and initial programming of the real-time data handling system, the facility will be usable for runway experiments.

A contract for the development of a laser tracker and integration of it with the radar is to be let in early 1973 with delivery, installation and checkout to be completed by the spring of 1974. An analysis of the laser eyesafety problem in this study concluded that present standards for maximum permissible exposure can be readily met with a laser tracking system. With the addition of the laser tracker to provide high precision, close-in tracking down to touchdown, the facility will have met the original goals.

It is planned that a C-band telemetry system utilizing the FPS-16 radar transmitter and receiver will be procured to serve as a general-purpose telemetry available to all users. The system will have both an up- and down-link capability and will be capable of transmitting both proportional (analog and digital) data and discrete commands. The ground-based part of the system will become an integral part of the FPS-16 radar system. Airborne components, consisting of an encoder and decoder to work in conjunction with conventional transponders, are to be furnished by users.

In addition to the C-band systems, other telemetry systems will be available, the most significant of which is the Piloted Aircraft Data System (PADS) being assembled at NASA LRC. PADS is a general-purpose on-board recording system, down-link, L-band, PCM telemetry system, and ground-based recording system.

The two major computational problems that remain to be resolved are the achievement of the capability to provide good rate data and the availability of suitable digital filters. Initial plans specified that rates were to be derived from position tracking data. Early efforts by NASA Wallops led to the

development, under contract, of a Kalman-type filter, designated KAPPA, which was formulated to automatically include rates as outputs.

A limited investigation of an initial form of KAPPA was conducted by the simulation of KAPPA in the role of providing position and rate data to the VTOL flight director being studied at NASA LRC with the CH-46 helicopter. In simulated level flight with KAPPA in the control loop and the filter parameters set near optimum, the aircraft flight appeared to be on the verge of instability. Open loop runs showed that lags in both position and rates on the order of one to two seconds are prevalent. A major disadvantage of KAPPA in this regard is the fact that its dynamic characteristics are highly dependent on conditions such as wind gusts, radar noise, and the system model--none of which is normally known precisely.

It should be emphasized that this analysis is based primarily on the application of KAPPA in a closed loop mode. No attempt has been made to assess the performance of the filter in other real-time or post-flight applications, and any implications as to the performance in other applications are not made. Furthermore, this report does not include any analysis of other filters available at Wallops, and no implications concerning the performance of KAPPA relative to other filters are intended.

An in-depth study of KAPPA has been undertaken at NASA Wallops for both real-time and off-line applications. Modifications intended to improve the filter for real-time applications are being made; however, no attempt was made during this effort to evaluate these modifications. The CH-46 simulation results using the initial form of KAPPA indicate that the insertion of the filter can cause adverse effects in the control loop; hence, it is recommended that before any version of KAPPA is used in a closed loop system, its effects on the system should be thoroughly assessed.

Since it appears doubtful that rate data of sufficient accuracy and with acceptable lags for all planned projects will be available by derivation from position tracking data, it is recommended that more direct means of measuring rate be investigated. It has been suggested that more accurate rate measurements can be obtained by supplying a Kalman-type filter (such as KAPPA) with additional rates and accelerations obtained from on-board sensors. Also, a pseudo-noise multilateration system is planned as an addition to the Wallops instrumentation in the near future. This system will provide extremely accurate rate data, and techniques should be investigated for using these rate data in runway-associated flight projects and in the real-time mode.

The laser eyesafety problem has been investigated for three representative laser tracking systems. It was concluded that any of these systems is adequate from the viewpoint of eyesafety over the anticipated laser-to-aircraft ranges.

Additional effort is desirable to continue to update system requirements and capabilities and to determine appropriate system tests for the complete radar/computer/telemetry complex. The overall system transfer functions in various modes should be determined for use by project personnel.

After system evaluation, a user-oriented report should be prepared with extensive documentation of the system capabilities and the various tracking/data processing options available to the user.

1.0 INTRODUCTION

Flight test evaluation of aeronautical system concepts undergoing research and development requires aircraft tracking instrumentation which is compatible with the accuracy and precision of the systems being studied. Flight research projects at NASA Langley Research Center (LRC) rely on the facilities at NASA Wallops Station for the majority of their flight testing. In recognition of the fact that newly-evolving systems place more exacting requirements on tracking systems, NASA has initiated efforts to upgrade the Wallops facilities to meet the demands.

The planned improvements in the Wallops runway facility consist of installation of a combined radar and laser tracking system along with real-time data handling and up- and down-link telemetry systems to provide a flexible facility for tracking and providing various types of guidance commands to aircraft.

The Research Triangle Institute (RTI) has participated in this program since its inception primarily in a liaison role between flight project managers at LRC and those responsible for facility improvement at Wallops.

An earlier RTI report (ref. 1) presented the basic requirements and original instrumentation plans for the facility. This report supplements the earlier report to present revised plans and new findings from studies as the system has evolved. There has also been recent interest from other aeronautical research agencies, such as the FAA and its contractors on the microwave landing system, in the use of the facilities at NASA Wallops Station. Since it is impractical to incorporate all of the new uses and requirements for additional instrumentation, this study has concentrated primarily on the radar/laser system complex and its associated data handing and telemetry system.

2.0 REVIEW OF REQUIREMENTS

2.1 Requirements Survey

As in previous phases of the contract, interviews were held with representatives of existing and planned flight research projects at LRC. Summary discussions of the findings in these interviews are given below. For those projects previously covered in ref. 1, the discussions focus on additions or refinements of previous results reported.

VTOL In-Flight Simulation with CH-46

Contacts: Mr. J. R. Kelly, Mr. F. R. Niessen and Mr. J. F. Garren

Summary: Testing will continue for several more years with the CH-46 helicopter. Requirements remain basically the same. Obtaining good rate data without lag is still of concern. A new on-board stable platform is being used with analog output Kalman filters to derive rates.

Real World Contact Analog Displays

Contact: Mr. Gene Moen

Summary: The original concept of positioning a TV camera over a relief, scale model has been changed to mounting cameras on the aircraft and to other schemes for generating displays. The latter will use the LRC Terminal Area Display Facility being assembled by Hatfield and Elkins. Initial tests have been concerned with VFR approach statistics and determination of basic aircraft characteristics.

Tracking data will be needed with the same accuracy requirements previously stated. The SH-3 will be the primary aircraft used.

Light STOL Terminal Area Approach and Airspace Requirements

Contact: Mr. H. L. Crane

Summary: Tests similar to those conducted with the Heliocourier are to be conducted with the Cessna Skymaster and possibly other aircraft. Data requirements are essentially the same as previously specified.

Aircraft Flyover Noise Tests

Contact: Mr. D. A. Hilton and Mr. R. E. Shanks

Summary: The original testing concept is to continue indefinitely using different types of aircraft with the same data requirements previously specified. Runway 10-28 will be the primary runway for touch-and-go runs and as a guide

for fly-bys. Typical speeds will be up to 200 knots. If angle tracking rates immediately abreast of the radar/laser system are too high, data for this portion of the runs can be sacrificed.

Terminal Area Navigation by Trilateration

Contact: Mr. C. W. Meissner

Summary: Tests are to be similar to those conducted by T. Ballard to compare trilateration data in real-time with radar tracking data. Accuracy requirements are the same as those previously specified.

STOL Crosswind Landing Operations

Contact: Mr. A. W. Hall

Summary: The purpose of the project is to extend crosswind landing limits to improve operational reliability and safety. The Twin Otter will be the primary aircraft used. Both ILS and VFR approaches are to be used on straight, segmented and curved approach paths. The only data needed in the aircraft are ILS signals. Tracking data will be needed throughout the run down to and including touchdown and roll-out. Good rate data at touchdown are needed. Previously specified data accuracies are adequate. Testing is to be done at various wind gust and shear conditions. All tests will be conducted under good visibility conditions.

Slot Spoiler for Direct Lift Control

Contact: Mr. Andrisoni

Summary: Testing is to be done to measure effects of slot spoiling. The Comanche (PA-24) will be used. Only conventional ILS signals will be needed by the aircraft. All runs are to be conducted with straight-on 3-6 degree approaches and all runs will terminate at touchdown. Position measurements are needed at touchdown to determine dispersion. Data accuracy requirements previously specified are adequate.

STOL/ATC In-Flight Simulation

Contact: Mr. R. H. Sawyer

Summary: The project is concerned with development of flight director capabilities for curved and segmented approaches. Radar coverage is needed out to 40 n mi. Tests will be run with the Twin Otter aircraft with glide slopes up to 7.5 degrees. The tests are to be tied in with FAA simulations

at NAFEC. Data to the aircraft will consist of command course and command bank angle for inputs to the flight director. Data accuracies previously specified are adequate.

Terminal Configured Vehicles & Avionics

Contact: Mr. R. T. Taylor and Mr. T. Walsh

Summary: The purpose of this project is to improve terminal area flight operations. Flight testing is planned with the Sabreliner and 737 aircraft with initial tests for aircraft capabilities and preliminary display requirements to start in mid-1973. Position and rate data will be needed through touchdown and roll-out and possibly on the ground. Data accuracies previously quoted are adequate. Data to the aircraft will require simulated ILS and MLS (microwave landing system) signals. Detailed requirements are currently being defined. Testing will eventually be done at night and in fog and rain conditions.

Terminal Area Display Facility

Contact: Mr. J. J. Hatfield and Mr. H. C. Elkins

Summary: The purpose of the system is generation of advanced, integrated cockpit 2-D and 3-D displays for in-flight and simulator evaluation. The facility is intended for support of several of the flight projects identified above that utilize displays in the aircraft. It accepts position and velocity data from the runway facility as well as telemetered data such as attitudes from the aircraft, and generates displays and guidance-related signals for transmission back to the aircraft. Display data are typically transmitted to the aircraft over a wideband FM/TV link. Previously specified accuracies of input data are acceptable. There is special concern for good rate data with minimal lag.

2.2 Summary of Requirements

Based on the interviews summarized in the preceding section, the basic requirements previously reported in ref. 1 remain unchanged. New projects that have evolved since the previous report have served to add stress to the demand for a high precision tracking capability down to touchdown and on the ground through roll-out, deceleration, and taxiing. Added emphasis has also been placed on the availability of good rate data.

3.0 REVIEW OF INSTRUMENTATION PLANS

Since the acquisition of the Wallops runway facility began, the basic system concept has remained the same as described in ref. 1. The purpose of this section is to review the plans and provide additional information where appropriate.

For reference purposes a system block diagram is presented in Fig. 3-1 which was taken from ref. 1. The combined radar and laser tracker provide tracking data to a real-time data handling system which also may receive data from aircraft systems via down-link telemetry and from other tracking systems. Output data from the data handling system can be recorded and supplied for real-time operation to other ground-based systems and to the aircraft.

A program schedule for the remaining acquisition activity of the system is shown in Fig. 3-2. The following sections will cover the schedules of individual items identified in Fig. 3-2.

3.1 FPS-16 Radar

The FPS-16 radar in the runway facility is a C-band, monopulse (amplitude comparison) radar having one (1) megawatt peak power. It is recalled that this particular radar differs considerably from most FPS-16 radars in that it has a 16 ft (rather than 12 ft) diameter antenna, a hydraulic-drive (rather than gear-drive) pedestal, and a digital (rather than analog) range servo. Many additional, more subtle design features were also incorporated in the design, and these are described in ref. 2. A picture of the radar is included on page 12.

A list of technical and performance characteristics for the radar is given in Table 3-1. It is also known that several field changes were made to the radar prior to its acquisition by NASA Wallops and for which documentation was not available. Users needing precise radar characteristics for project planning and data analysis should contact NASA Wallops radar personnel for actual values of parameters in question. Additional changes to the radar have been considered from time to time. For example, it has been suggested by one LRC project manager that the range data output resolution be changed from 2 yds to 1 yd and by another that a Doppler system be added. Such changes have not been officially analyzed and planned. The addition of an attenuator

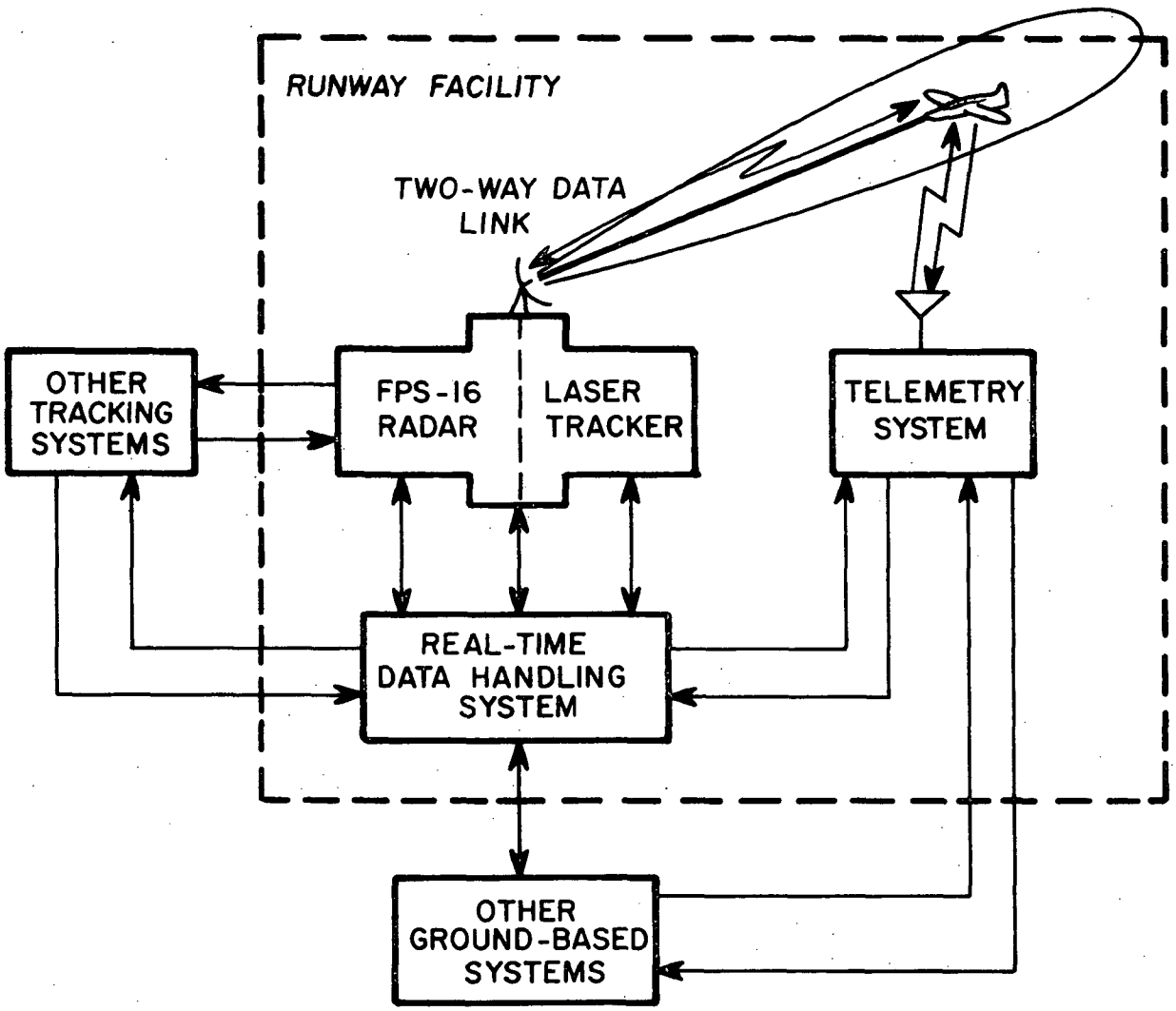

Fig. 3-1. Planned NASA Wallops Runway Facility.

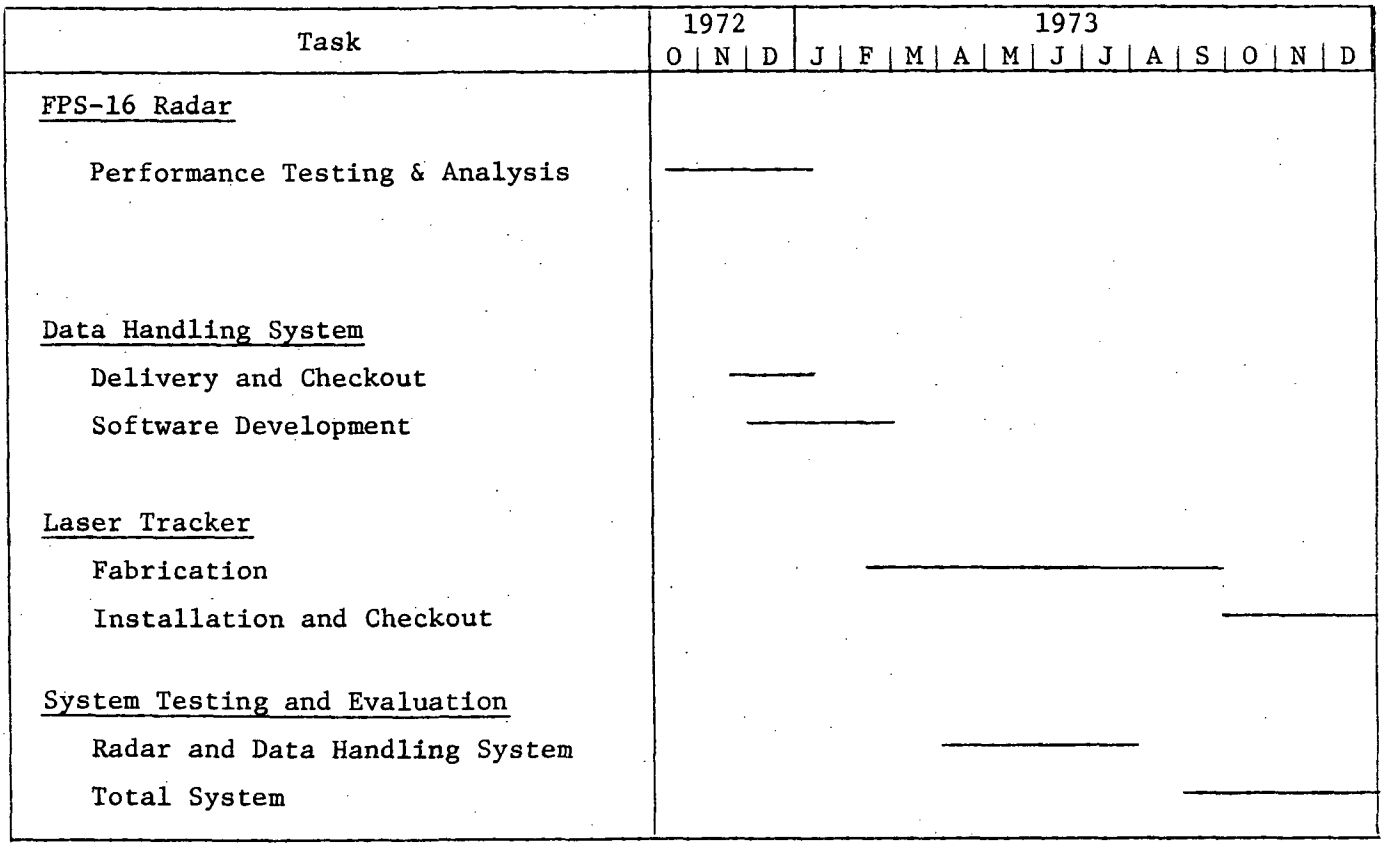

Fig. 3-2. Program schedule for Wallops Runway Facility.

Fig. 3-3. The FPS-16 radar for the NASA Wallops runway facility.

Table 3-1

Summary of Characteristics for the FPS-16 Radar

Transmitter	
Frequency range	5450 to 5825 Mc, continuously tunable
Peak power output	1 Mw
Nominal pulse widths	0.25, 0.50, 1.00 microsecond
Pulse repetition rates	160-, 640-, and 1024-pps rates are wired to three console pushbuttons. Three additional pulse repetition rates can be wired for console selection
Duty cycle	0.0011 maximum (any combination of PRF and pulse width that exceeds this value is disallowed)
Pulse coding	up to five 0.25-microsecond pulses per repetition period with minimum leading edge spacing of 1.0 microsecond (pulse-to-pulse variation in any pulse group < 1.0 db)
Power programming range	20 db minimum, either automatically controlled by the range tracker as a function of target range or manually controlled by the console operator
Built-in test equipment	power monitor
Antenna and Multimode Feed	
Main reflector	16-foot diameter paraboloid of revolution with a f/D of approximately 0.3
Subreflector	18-inch diameter hyperboloid of revolution mounted on a quadripod structure with its focus coincident with that of the paraboloid
Polarization modes	transmit and receive linear vertical or transmit left-hand circular and receive right-hand circular (selectable from console)
Gain	46 db minimum
Beamwidth	$0.71° \pm 0.04°$
Reference channel and error channel sidelobes	attenuated 18 db relative to the radiation intensity at the peak of the main lobe (refer to Acceptance Testing)
Error pattern depth of null	down at least 35 db from reference pattern peak

Table 3-1. Continued.

Pedestal	
Type of mount	2-axis, azimuth and elevation
Rotation limits:	
Azimuth	continuous
Elevation: Tracking	-10° to +90°
Boresighting	-10° to +190°
Drive	hydraulic valve-motor; two in azimuth, one in elevation
Power gear train:	
Azimuth	dual aiding with mechanical pre-load
Elevation	single pivoted low backlash
Main bearing:	
Azimuth	hydrostatic
Elevation	ball and roller
Receivers	
Noise figure	4.5 db (with parametric amplifier)
Dynamic range	73 db
Intermediate frequency	30 Mc
IF bandwidths	2.2 $\pm$ 0.5 Mc and 9.0 $\pm$ 1.4 Mc (selectable from console)
Angle Servos	
Maximum tracking velocity:	
Azimuth	800 mils/sec in winds up to 45 knots 650 mils/sec in winds up to 60 knots
Elevation	450 mils/sec in winds up to 45 knots 650 mils/sec in winds up to 60 knots
Maximum tracking acceleration:	
Azimuth	1.3 rad/sec^2 in winds up to 45 knots 1.0 rad/sec^2 in winds up to 60 knots
Elevation	1.3 rad/sec^2 in winds up to 45 knots 0.6 rad/sec^2 in winds up to 60 knots
Track bandwidth selections	0.5 to 2.5 cps
Track velocity constants	infinite
Track acceleration constants	0.6 to 16 sec^{-2}

Table 3-1. Continued.

Acquisition	digital computer or analog (single 1:1 speed synchro)
Scan patterns	circle, spiral, raster, rectangular in either digital or analog acquisition
Range Tracker	
Measurement interval	500 yd to 32,000 n. mi. (expandable to less than 300 ft with beacon delay and to 256,000 n. mi.)
Output data word length	25 bits
Output data granularity	1.953 yd/bit
Velocity tracking capability	20,000 yd/sec
Acceleration tracking capability	20,000 yd/sec^2
Slew rate	240,000 yd/sec, maximum
Velocity constant (Kv)	infinite (type II servo)
Acceleration constant (Ka)	$2500/sec^2$
Master oscillator stability	1×10^{-8} parts/day
Internal random error	3 yd RMS (S/N of 18 db)
Probability of detection (multiple gate array)	99.9% in 30-millisecond interval with a S/N of 10 db at PRF of 640 pps and a false-alarm probability of 10^{-4} on a target moving at 20,000 yd/sec
Data Subsystem	
Angle encoders (azimuth and elevation)	
Type	2-speed mechanical-optical
Mechanical encoder output	5-bit Gray-code word
Optical encoder output	13-bit Gray-code word
Redundancy	LSB of the mechanical encoder and the MSB of the optical encoder are redundant
Angle resolution (granularity)	0.0488 mil/bit
Output digital data	
Readout rate	10, 20, or 40 samples/sec
Shift rate	100,000 bits/sec

Table 3-1. Continued.

Shift order	serial, LSB first
Data form	non-return-to-zero (NRZ) with LSBs aligned
Azimuth word	17-bit binary
Elevation word	17-bit binary
Az and El offset word	8-bit binary for Az offset; 8-bit binary for El offset
Range word	25-bit binary
Angle error and AGC word	8-bit binary for AGC voltage; 8-bit binary for Az error; 8-bit binary for El error
Identification word	10-bit word (3 bits are provided as spares) for computer program control
Input digital data	
Range-designation word	21-bit binary
Az and El designation word	10-bit elevation error word; 1-bit for El servo gain; 10-bit azimuth error word; 1 bit for Az servo gain; 3 bits reserved for possible automatic bandwidth control
C-scope word	8-bit elevation deflection; 8-bit azimuth deflection
Stabilized Az word	17-bit binary
Stabilized El word	17-bit binary
Range rate word	15-bit binary
Synchro data outputs	
Azimuth (coarse)	360°/revolution
Elevation (coarse)	360°/revolution

Supplementary inputs and outputs:

The Radar Data Junction Box (Cabinet 180) provides a centralized location for the radar interface with other systems. Digital data lines, video signals, synchro signals, relay contact closures, etc., are all available at the Radar Data Junction Box for external distribution. Volume 8 of the Technical Manual for Radar Set Model AN/FPS-16(V) contains a complete listing of all the available signals.

Volume of Coverage

Range coverage	up to 32,000 nautical miles
Angle coverage	
Elevation	-10° to +90°
Bearing	360°

Table 3-1. Continued.

Measurement Accuracies

(On targets with signal-to-noise ratio of at least 18 db, within ± 1/4 beamwidth about the beam axis, and after error correction is performed.)

Angle error*	1 - σ value
Random component (above 5 cps)	0.1 mil or less
Cyclic component (between 0.01 and 5 cps)	0.1 mil or less
Systematic component (below 0.01 cps)	0.1 mil or less
Range error**	
Random component	15 ft or less
Cyclic component	10 ft or less
Systematic component	15 ft or less

Angle Acquisition Aids

Auxiliary angle tracking (Auxtrack)	
Acquisition range	either the full range of operation or within a 40K yd interval gate
Probability of acquisition	99.5% or better in 0.2 seconds on a target having a 10-db S/N as measured at the IF output
Antenna scans	
Circle	circle diameter adjustable from 1 to 6 degrees
Spiral (concentric circle)	diameter of spiral adjustable out to 5.5 degrees
Raster	2.4 by 8 degrees (major axis in either Az or El coordinate)
Rectangular	0.6 by 8 degrees (major axis in either Az or El coordinate)
Range acquisition aid	
Digital detection with multiple gate array	
Number of gates	20

*Exclusive of all atmospheric and multipath effects.
**Exclusive of beacon delay and velocity of propagation errors.

Table 3-1. Concluded.

Required designation accuracy	± 10,000 yards
Probability of acquisition (for 30-millisecond interval)	99.9% with a S/N of 10 db and a false alarm probability of 10^{-4} on a target moving at 20,000 yd/sec.

(40-60 db) to the receiver has been initiated to provide the capability to track to the minimum specified range of 500 ft.

It was also noted in ref. 1 that the 17-bit angle data output word length does not conform to the 19-bit requirement given in that document. Plans for changing the angle encoders to provide a 19-bit readout have not been made. Wallops has determined that the change will be more extensive than originally thought, requiring considerable modification to the electronics in the digital data handling subsystem of the radar.

Installation of the FPS-16 radar has proceeded on schedule and is now complete. The runway facility cannot be considered fully operational, however, until adequate provision is made to supply and process output data. As shown in Fig. 3-1, the major means of data output and processing is through the real-time data handling system which is scheduled for delivery and checkout in early 1973. Without this means of data output the radar is of limited utility for some runway operations; however, when the data handling system is available and operational, the combined radar and data handling system will have extensively better capability than the presently-used GSN-5 system.

Location of the radar at NASA Wallops is as specified in ref. 1: adjacent to Building A-41, northeast of the intersection of runways 10-28 and 18-34, approximately 500 ft. from the centerline of both runways. The radar electronics and control console are housed in Building A-41. Additional area alongside the radar building has been paved for parking instrumentation vans, and electrical power outlets and signal cable trays are to be provided.

Measurement accuracies of 0.1 mil (1σ) or less in angle and 15 ft. (1σ) or less in range given in Table 3-1 are consistent with values previously quoted. Tracking tests at NASA Wallops are being initiated whereby satellite tracking data from the runway FPS-16 radar are to be compared with simultaneous tracks with the FPS-16 and FPQ-6 radars on Wallops Island. Additionally, it is recommended that aircraft tracking tests be conducted after delivery of the data handling system to determine accuracies under conditions more closely related to runway operations.

3.2 Laser Tracker

A laser tracker is planned for the runway facility to provide a high precision tracking capability at close-in ranges down to touchdown and on the ground. As described in ref. 1, the laser is to be mounted on the FPS-16 radar antenna with the laser beam boresighted parallel to the radar boresight axis. Radar tracking will thus aid laser acquisition as the aircraft gets within laser range. After angle acquisition, the laser will provide the pointing error signals to the radar angle servos. The laser will, however, have a separate range tracking system.

Procurement specifications prepared by NASA Wallops generally conform to the requirements and instrumentation plan given in ref. 1. Table 3-2 lists some of the key performance specifications of the laser. Specific functional capabilities specified for the combined radar and laser tracker system are:

Automatic range and angle tracking on passive, cooperative targets in the Laser Mode;

Automatic range and angle tracking on cooperative and noncooperative targets in the Radar Mode;

Simultaneous automatic range tracking by the laser and radar range systems;

Manual acquisition in range and angles in either the Laser Mode or the Radar Mode;

Automatic handover from Radar Mode to Laser Mode; and

Automatic handover from Laser Mode to Radar Mode.

System performance specifications issued for procurement are rigid; however, considerable leeway was afforded to the prospective supplier in terms of hardware and functional design features such as laser type and method of scanning to meet system requirements. A digital range servo was specified to make the data readout timing consistent with the existing capability.

Power programming of the laser transmitter was specified to assure eye safety of the pilot and other crew members of the aircraft being tracked. During laser tracking, the power is programmed as a function of laser range. During laser acquisition, the radar range is used to control the laser power output. During a range coast mode, the laser power programming will be dependent on a velocity memory circuit; however, if after 5 sec the radar or

Table 3-2

Major performance specifications for the laser tracker.

Range Tracker	
Measurement interval	350 ft to 120,000 ft
Output data word length	25 bits maximum
Velocity tracking capability	10,000 ft/sec maximum
Acceleration tracking capability	2500 ft/sec^2 maximum
Slew rate	10,000 ft/sec maximum
Measurement accuracy	0.3 ft rms for ranges from 350 ft to 10,000 ft
	0.003% of range rms for ranges from 10,000 ft to 36,000 ft
Range data output LSB	$\leq$ 0.5 ft
Servo bandwidths	at least four in number over a decade
Angle Error Detector	
Angle coverage[/1]	-10 deg to +90 deg elevation 0 to 360 deg azimuth
Velocity tracking capability[/1]	450 milliradians/sec
Acceleration tracking capability[/1]	acceleration created by fly-bys giving the maximum velocity capability
Precision[/2]	0.1 milliradians rms for ranges between 350 ft and 36,000 ft
Radar to laser handover time	less than 2 sec for ranges greater than 4000 ft.

/1 This capability is listed for the laser tracker exclusive of its integration with the radar system.

/2 This capability refers to the angle pointing error signal supplied to the radar angle servos.

laser has not reacquired, the laser power programmer will automatically return to maximum attenuation (minimum power output). Fail-safe features are included to assure that accidental overexposure of personnel to laser radiation does not occur.

Three retroreflector packages are included in the laser tracker procurement. The retroreflectors will serve as passive, cooperative tracking aids similar to radar corner reflectors. The weight and volume of the retroreflector packages are specified not to exceed ten pounds and 0.5 cu ft, respectively.

3.3 Real-Time Data Handling System

The real-time data handling system is a computer complex that receives and processes data in real-time from the FPS-16 radar and from other possible sources (including aircraft) via data links, other radars, and other ground-based systems. Output can be supplied from the system back to the aircraft via telemetry, to recorders and displays, and to other ground-based systems.

Plans for acquisition of the data handling system have changed considerably from those described in ref. 1. The UNIVAC 1218 system never materialized as an interim system because of problems in acquiring a real-time interface. Rather, emphasis was placed on acquisition of the permanent, operational system. A contract for the system is near completion with delivery expected in the first quarter of 1973.

A block diagram of the real-time data handling system is given in Fig. 3-4, which was taken directly from the procurement specification (ref. 4). In addition to the computer, computer peripherals, and input/output interface equipment shown, the system procurement included a software package consisting of a FORTRAN compiler, an assembler, a library of standard functions and operations, and various operational and maintenance programs such as read-in, read-out, diagnostic, debug, and dump routines. Operational software to include digital filters, glide slope and localizer error computations, display functions, etc., are not included but will be supplied separately by NASA Wallops.

Note that the system will be capable of accepting data simultaneously from the FPS-16 and several other radars and sources via remote registers, synchro-to-digital converters, and an FSK data receiver. Input data sampling rates will be selectable up to forty samples per second, the maximum output rate of the FPS-16 radar.

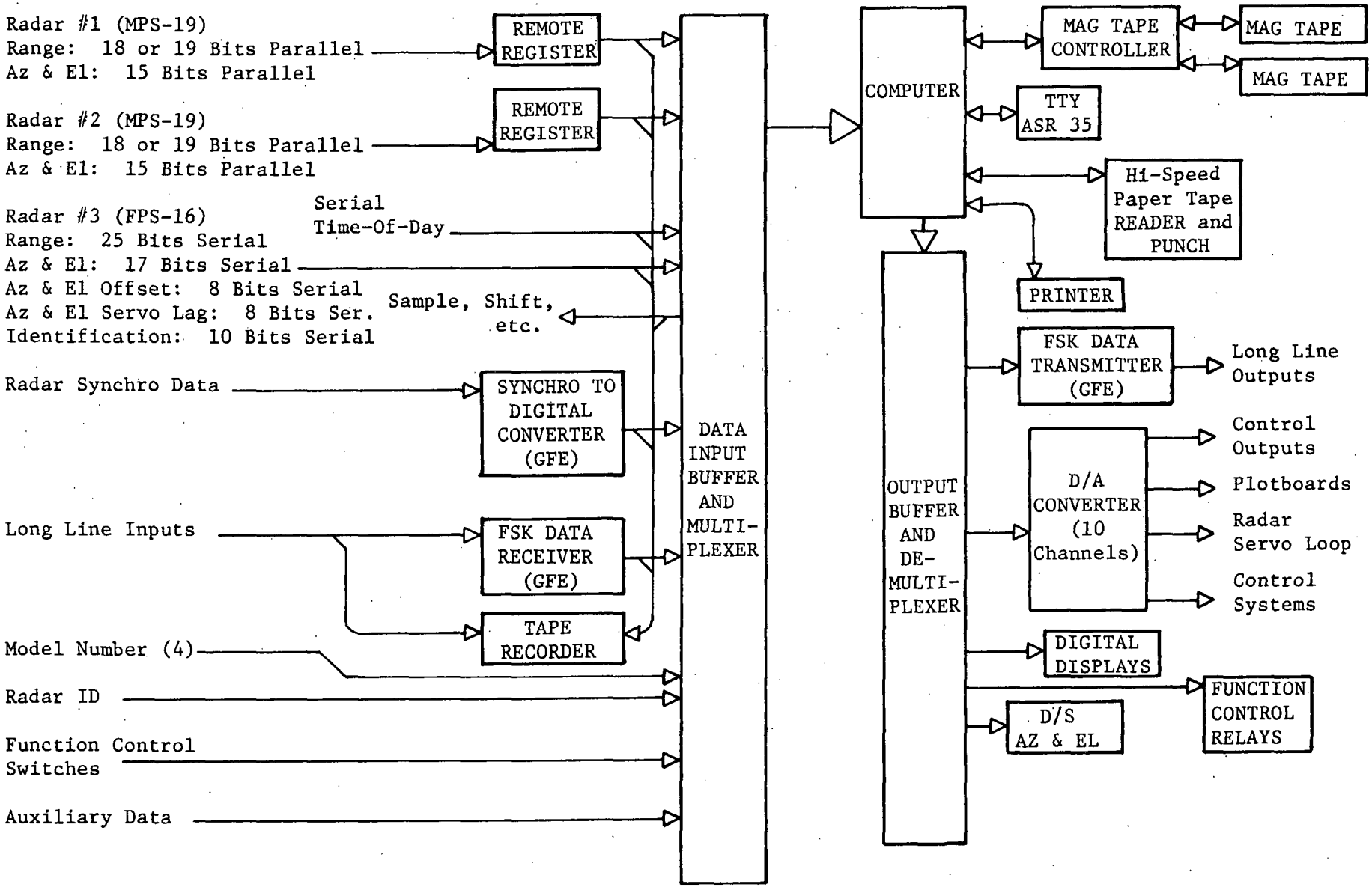

Fig. 3-4. Experimental runway facility data system block diagram.

The computer for the system will be a Honeywell H316, salient features of which are:

Memory Size: 16 K words (expandable to 32K)

Memory Cycle Time: 1.6 μsec.

Word Length: 16 bits

I/O Word Transfer Rate: 250 KHz

Memory Address: Direct.

Double precision computations are presently accomplished by software; however, double precision hardware is available for this computer and is being considered. Floating point hardware is provided.

The output buffer and demultiplexer has a capacity of 43 data channels, six of which provide 25-bit serial data back to the FPS-16 radar. The unit is also expandable to 64 channels. The digital-to-analog converters are specified as 13-bit, 0.01% accuracy units.

Additional details of the data handling system are given in the procurement specification, ref. 4. Additional documentation on the system capability will be available after delivery of the system.

3.4 Telemetry

Extensive telemetry capability will be needed for the runway facility to transfer data to and from aircraft. Several systems are anticipated to encompass the needs of all experimeters. The following summarizes typical systems that are available or are being considered.

ILS Signal Generation and Transmission

The VHF and UHF units now used for transmitting the ILS-type signals were described in ref. 1. These units are located in the GSN-5 radar van. The transmitters will most likely remain located in the GSN-5 radar van while the GSN-5 is in operational status.

C-Band Telemetry

A C-band telemetry system that utilizes the FPS-16 radar and airborne C-band transponders is planned. This system will serve as a general-purpose up- and down-link telemetry system readily available to all users. Acquisition of the system is still in the budgeting stage; however, rapid delivery of the system is expected when procurement is initiated, as such systems are available

commercially as off-the-shelf items and installation is essentially a matter of making simple cable connections.

One such system is the Vega Command and Data System, consisting of the Model 642 Interrogation System (for the up-link) and Model 643 Data System (for the down-link) manufactured by Vega Precision Laboratories, Inc. (ref. 5). A block diagram of the system is given in Figure 3-5.

Both the up-link and down-link portions of the system can handle both proportional (analog or digital) data and discrete commands. The information is transmitted by triggering the radar or transponder transmitter to transmit three additional pulses before (for the up-link) and after (for the down-link) the transmitter "main bang" pulse while the radar continues to track on the main bang pulses. Pulse position coding (PPC) of pulses in each pulse group of four pulses associated with each main bang provides a channel identification and coding of the information. Discrete commands are transmitted by generating and detecting the data pulse within a very narrow (~2 μsec) window. Proportional data are transmitted by assigning and measuring the position of the data pulse within a wide window (~100 μsec).

For planning purposes, potential users of the C-band telemetry system may assume the following characteristics:

For the up-link:

No. of proportional channels: up to 16
No. of discrete channels: up to 64
Update rate: programmable within limits of system capability
No. of bits: 10 per sample
Proportional range: $\pm$ 10 v.
Resolution: 1 in 2^{10} (~0.1%)
Accuracy: $\pm$ 0.5%

For the down-link:

No. of proportional channels: up to 16 (expandable to 48)
No. of discrete channels: up to 64
Update rate: programmable within limits of system capability
No. of bits: 10 per sample
Proportional range: $\pm$ 10 v.
Resolution: 1 in 2^{10} (~0.1%)
Accuracy: $\pm$ 0.5%

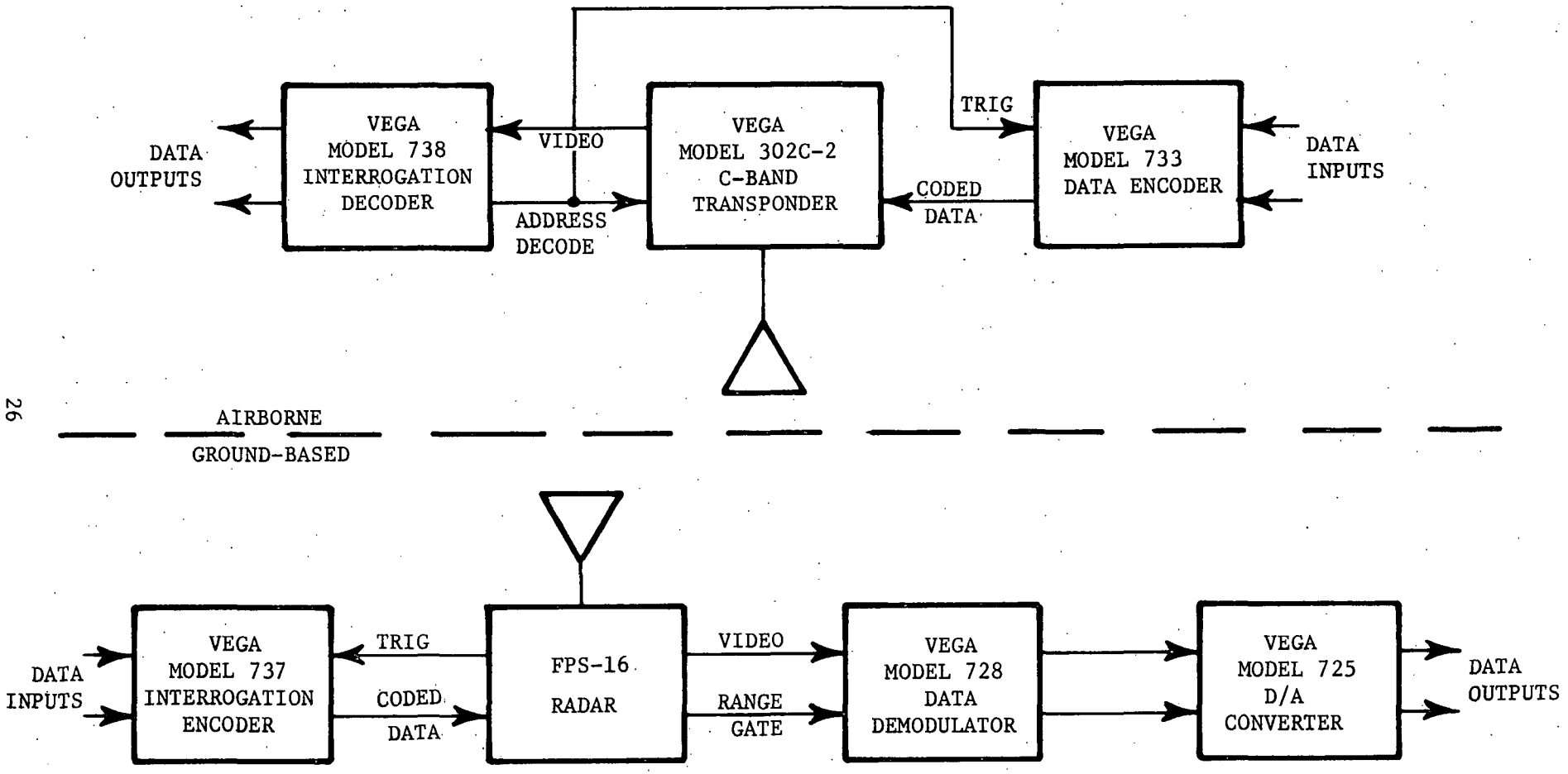

Fig. 3-5. System block diagram, Vega command and data system.

It is noted that trade-offs will exist between the number of proportional and discrete channels versus channel update rates. Basically, the update rates will be determined by (Radar PRF/No. of channels) within certain limitations. The maximum proportional channel update rate for the Vega system is PRF/16. This is attainable if only eight proportional channels are used. Proportional channel update rates are generally limited to 40 samples/sec or an information bandwidth of about 20 Hz. It is recommended that the potential user contact S. Sokal, FID, NASA LRC for up-to-date specifications on update rates if needed.

Because of radar duty cycle limitations the maximum operating PRF with the C-band telemetry system will be 640 Hz.

Some experimenters will need near maximum data rate capability of the system in terms of number of channels and bandwidth which will require operating the radar at maximum PRF. A PRF of 1280 (or pulse-to-pulse spacing of 780 μsec) is achievable with the FPS-16 with minor wiring changes (ref. 2). The normal unambiguous radar range for this PRF is about 65 n. mi. Because of the additional time in the PRF cycle required for the data pulses, 176 μsec maximum for proportional channels (ref. 5), the unambiguous radar range will be reduced to about 50 miles for one-way transmission and to about 35 miles for two-way transmissions. This range capability will be more than adequate for planned uses of the runway facility. Because of the pre- and post-trigger methods of generating the data coding pulses for the radar and airborne transmitters respectively, the minimum range is expected to be less than 500 ft.

Piloted Aircraft Data System (PADS)

PADS is a combination on-board data recording, L-band down-link telemetry, and ground-based data recording system being assembled at NASA LRC under the direction of V. H. Knight, Jr., FID. PADS utilizes both PCM and FM with 32 to 104 channels (programmable in groups of eight) of on-board PCM recording capability and 5 to 40 channels of on-board FM recording capability. The quantization of the PCM is 9 bits (1 in 512 resolution) and the resolution for FM is 2 to 3 percent. All of the PCM channels can be transmitted to the ground at a maximum rate of 90 K bits/sec along with up to 10 of the FM channels. The range coverage of the system is approximately 60 n. mi.

Four airborne systems and two ground stations are being assembled. It is planned that one ground station will be located at NASA Wallops and the other at NASA LRC.

Complete technical documentation on the system will not be available

until mid-1973. It is recommended that potential users contact the project manager for technical details until the system description is available.

FM/FM Telemetry

A ten channel UHF FM/FM system for up-link transmissions of analog data has been in use for several years by the CH-46 project. Depending on the needs of a project, this system could be used to supplement other systems such as the C-band system and PADS. J. Bryant, FID, NASA LRC, is the cognizant engineer for this system.

Wideband System

A wideband, S-band FM/TV system is available for ground-to-air transmission of continuous video-type signals. This system will be an integral part of the LRC Terminal Area Display Facility under the cognizance of J. Hatfield and H. Elkins (see Sec. 2.1). The system has a maximum video baseband of 25 MHz, thus will provide considerable flexibility for transmitting wideband signals.

NASA Wallops Telemetry Capability

An extensive complement of telemetry receiving equipment exists at NASA Wallops which can be made available for runway operations. A permanent, S-band PCM facility is housed in Building N-162 which can receive and process 32 analog channels. Additional wideband equipment, VHF, and L-band equipment are also available. The potential user can contact W. H. West at NASA Wallops concerning specific capability information and for technical assistance in providing needed telemetry receiving equipment.

3.5 Supplementary Systems

As a result of revised flight research plans and additional uses anticipated for the runway facility, additional instrumentation and capabilities will be available at NASA Wallops. Although the scope of this effort was not able to encompass all the detailed requirements and plans, the following briefly describes these supplementary systems for informational purposes.

It is planned that prototypes of the microwave landing systems being developed under sponsorship of the FAA will be installed for evaluation studies at NASA Wallops. In connection with the evaluation of these systems, the GSN-5 and MPS-19 radars are to be retained indefinitely and will continue to be available for other flight research projects. These radars are also to be modified to provide digital outputs.

A new flight control center is under construction which will be located in the present control tower building. A full complement of displays and plotters will be provided in the control center. Flight project representatives will have access to the facility for overseeing and supervising flight tests.

A data link between NASA LRC and NASA Wallops is planned which will permit facilities at both installations to be linked together for real-time applications. For example, tracking data generated at NASA Wallops can be supplied over this link, when available, to real-time air traffic control simulations on the computer at NASA LRC. Requirements, instrumentations, schedules, and funding are currently being determined.

NASA Wallops plans to have available a data link between the real-time data handling system and the GE-625 computer. Flight researchers will thus be able to perform more extensive computations in real-time than could be done only by the H316 computer being provided with the runway facility. The potential user should be aware, however, of possible time delays of 0.2 sec. or more to transfer the data back and forth between computers over the FSK system to be used.

Procurement action has been initiated for hardware to construct an experimental multilateration system for air navigation studies at NASA Wallops. The extent to which this system will be generally available as a supplementary tracking system is unknown at present.

4.0 SPECIAL PROBLEM INVESTIGATIONS

4.1 Software Evaluation

NASA Wallops has contracted for the development of a digital filter for use in the runway facility. This algorithm, designated "KAPPA" (Kalman Program for Positioning Aircraft), is described in detail in ref. 6. A brief study of KAPPA has been included as a part of this program in an attempt to ascertain its applicability to Langley flight research projects. This section describes that study and includes a summary description of KAPPA as well as preliminary results obtained by computer simulation of KAPPA in a realistic flight research environment.

4.1.1 KAPPA Description

As implied by its name, KAPPA employs a (discrete) Kalman-type formulation. The KAPPA algorithm currently exists in a "basic" form with additional options available dependent on user requirements. Emphasis here will be directed to the basic form, while the options will be briefly described for completeness.

4.1.1.1 The Discrete Kalman Filter

The discrete Kalman filter is formulated under the following conditions. First, the true state sequence (signal) observed in the presence of noise can be modeled as a finite order difference equation driven by a random forcing function which is zero mean white-Gaussian noise with known covariance. Second, this sequence is measured in the presence of additive white-Gaussian noise with known covariance. The foregoing can be viewed schematically as shown in Fig. 4-1, or mathematically as

$$X_n = \Phi_{n/n-1} X_{n-1} + \Gamma_n W_n \tag{4-1}$$

$$Y_n = M_n X_n + V_n \tag{4-2}$$

where W_n is zero mean white-Gaussian noise (disturbance) with covariance "Q_n",
Γ_n is the disturbance response matrix,
X_n is the value of the state at time "n",
$\Phi_{n/n-1}$ is the process transition matrix from time "n-1" to time "n",
M_n is the measurement constraint matrix,

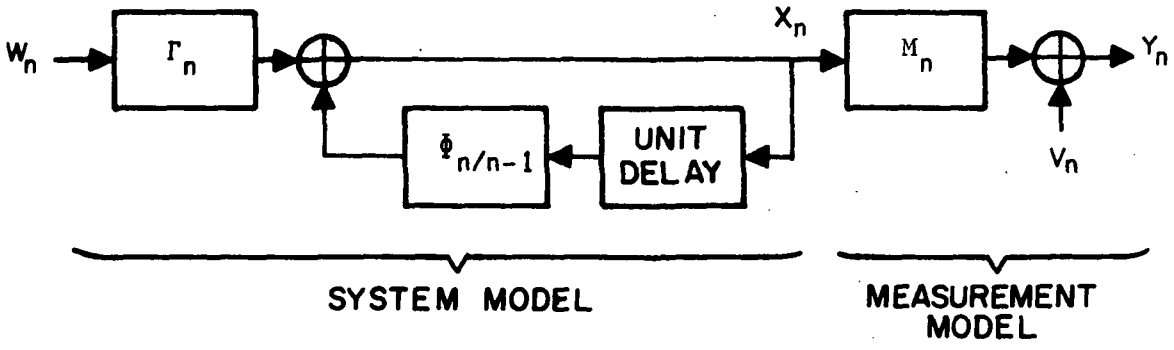

Fig. 4-1. Schematic representation of model(s).

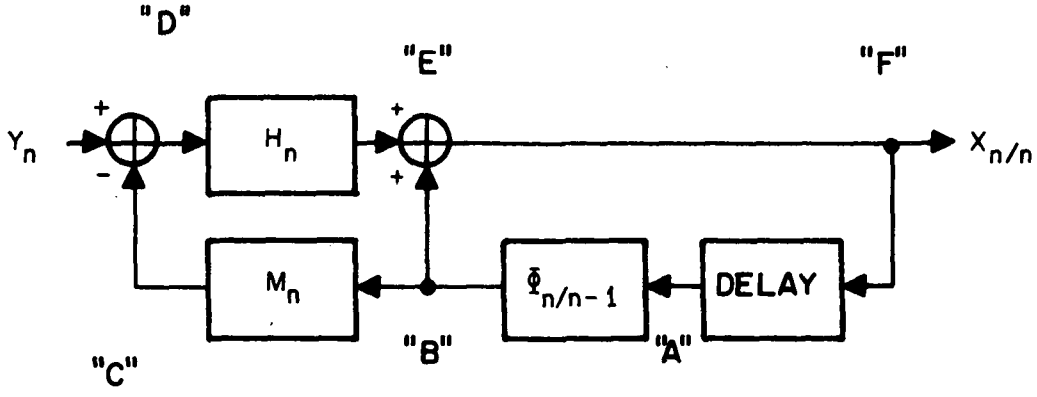

Fig. 4-2. Discrete Kalman filter.

V_n is zero mean white-Gaussian measurement noise with covariance "R_n",
and Y_n is the measurement (data) at time "n".

With the formulation above, it can be shown (ref. 9) that the optimal estimate (in the sense that the mean square error between the true signal and its estimate is minimum) can be obtained as:

$$X_{n/n} = \Phi_{n/n-1} X_{n-1/n-1} + H_n [Y_n - M_n X_{n/n-1}] \tag{4-3}$$

with

$$H_n = S_{n/n-1} M_n^T [M_n S_{n/n-1} M_n^T + R_n]^{-1}$$

$$S_{n/n-1} = \Phi_{n/n-1} S_{n-1/n-1} \Phi_{n/n-1}^T + \Gamma_n Q_n \Gamma_n^T$$

$$S_{n/n} = [I - H_n M_n] \, S_{n/n-1}$$

$$X_{0/0} = 0$$

$$S_{0/0} = S_0 \text{ (i.e., known)},$$

where H_n is the "measurement residual" gain (or weighting) matrix,
$S_{n/n-1}$ is the mean square error at time "n" conditioned on n-1 measurements (i.e., a predicted error covariance),
$S_{n/n}$ is the mean square error at time "n",
I is the identity matrix,
S_0 is the estimated initial condition on $S_{0/0}$,
$X_{n/n-1}$ is the estimate of the sequence at time "n" conditioned on n-1 measurements (i.e., a predicted estimate), where
$X_{n/n-1} = \Phi_{n/n-1} X_{n-1/n-1}$, and
$X_{n/n}$ is the estimate at time "n."

This can be viewed schematically as shown in Fig. 4-2.

An overview of the filter operation is as follows. Assume the filter has been properly initialized and is cycling; thus at point "A" one has an estimate of the signal $X_{n-1/n-1}$. Multiplication by the transition matrix will produce a prediction of the signal expected on the next iteration at point "B." This prediction of the signal is used (i.e., multiplied by the measurement constraint matrix M_n) to provide a noise-free prediction of the measurement expected on the next iteration at point "C." The predicted

measurement is compared with the actual measurement Y_m and a residual measurement error formed at point "D." This error is weighted by the gain matrix H_n (derived from the time-varying statistics of the model, measurement noise, and mean square error achieved on the previous iteration) and used to update the predicted signal (point "B") at point "E" to achieve the new estimate $X_{n/n}$ at point "F." The new estimate is delayed and the recursive action of the filter continued. Notice that the filter is simply the system model with error feedback.

4.1.1.2 Basic KAPPA

Basic KAPPA adopts an eight-dimension state space with position and rate along the principal axes of a cartesian coordinate system, acceleration, and tangent of bank angle as state variables. The origin of this coordinate system may be specified by the user. The system model equation

$$X_n = \Phi_{n/n-1} X_{n-1} + \Gamma_n W_n$$

is shown in expanded form as equation (4-4) to indicate the state vector and the elements of the transition matrix

$$\begin{bmatrix} x_n \\ y_n \\ z_n \\ \dot{x}_n \\ \dot{y}_n \\ \dot{z}_n \\ A_n \\ \Omega_n \end{bmatrix} = \begin{bmatrix} 1 & 0 & 0 & \Delta t & 0 & 0 & \frac{\Delta t^2}{2V}\dot{x}_{n-1} & \frac{\Delta t^2 g}{2V}\dot{y}_{n-1} \\ 0 & 1 & 0 & 0 & 0 & 0 & \frac{\Delta t^2}{2V}\dot{y}_{n-1} & -\frac{\Delta t^2 g}{2V}\dot{x}_{n-1} \\ 0 & 0 & 1 & 0 & 0 & 0 & \frac{\Delta t^2}{2V}\dot{z}_{n-1} & 0 \\ 0 & 0 & 0 & 1 & 0 & 0 & \frac{\Delta t}{V}\dot{x}_{n-1} & \frac{\Delta t g}{V}\dot{y}_{n-1} \\ 0 & 0 & 0 & 0 & 1 & 0 & \frac{\Delta t}{V}\dot{y}_{n-1} & \frac{\Delta t g}{V}\dot{x}_{n-1} \\ 0 & 0 & 0 & 0 & 0 & 1 & \frac{\Delta t}{V}\dot{z}_{n-1} & 0 \\ 0 & 0 & 0 & 0 & 0 & 0 & 1 & 0 \\ 0 & 0 & 0 & 0 & 0 & 0 & 0 & 1 \end{bmatrix} \begin{bmatrix} x_{n-1} \\ y_{n-1} \\ z_{n-1} \\ \dot{x}_{n-1} \\ \dot{y}_{n-1} \\ \dot{z}_{n-1} \\ A_{n-1} \\ \Omega_{n-1} \end{bmatrix} + \Gamma_n W_n \quad (4\text{-}4)$$

The system model selected for KAPPA represents a standard three-dimensional kinematic expression of a point mass moving at piecewise constant acceleration (with the exception of the bank angle term). Other dynamic models can easily be implemented; however, this study has concentrated on the model shown. This form is considered to be a viable compromise between an adequate description of aircraft dynamic behavior and computational complexity. Note that the transition matrix, and thus the Kalman gain matrix, are time-varying and that coupling exists between state variables.

Basic KAPPA accepts observations (in the case of utilization with the FPS-16) in radar (range, azimuth, and elevation) coordinates. This requires a polar-to-cartesian transformation (T_n) prior to input to the basic algorithm. This transformation is an integral portion of the form of KAPPA studied during this program. The observation equation

$$Y_n = M_n X_n + V_n$$

is shown in expanded form as equation (4-5) to indicate the requirement for this transformation and the form of the constraint matrix M_n.

$$T_n \cdot \begin{bmatrix} R_n \\ Az_n \\ El_n \end{bmatrix} = \begin{bmatrix} 1 & 0 & 0 & 0 & 0 & 0 & 0 & 0 \\ 0 & 1 & 0 & 0 & 0 & 0 & 0 & 0 \\ 0 & 0 & 1 & 0 & 0 & 0 & 0 & 0 \end{bmatrix} \begin{bmatrix} x_n \\ y_n \\ z_n \\ \dot{x}_n \\ \dot{y}_n \\ \dot{z}_n \\ A_n \\ \Omega_n \end{bmatrix} + T_n \cdot \begin{bmatrix} \varepsilon_R \\ \varepsilon_{Az} \\ \varepsilon_{El} \end{bmatrix} \qquad (4\text{-}5)$$

Notice that the constraint matrix is time-invariant and will result in no information regarding the last five states being contained in the radar observations. Also note that the radar error (measurement noise) covariance matrix also requires transformation prior to being input to KAPPA.

For an aircraft, the disturbance vector W_n would typically represent wind gust disturbances, and Γ_n the response of the aircraft to these disturbances. KAPPA, however, further formulates that W_n represent all unknown effects in the model and that $\Gamma_n = 1$. For example, ref. 6 recognizes that the transition matrix shown is not a perfect description of all aircraft systems. It then assumes that W_n contains the uncertainty introduced by unmodeled parameters in the true system model. One of the optional features (to be discussed) describes an approach to estimating the magnitude of the error introduced by unmodeled parameters.

4.1.1.3 Optional Features of KAPPA

In ref. 6, several optional features of KAPPA are described. The major ones of concern in this report are:

1. a sequential prefilter which cycles at the radar output data rate and permits sampled outputs to be delivered to KAPPA at a lower rate,

2. an adaptive bandwidth feature which increases the bandwidth of KAPPA during presumable transient conditions, and

3. an algorithm for computing the effects of parameters not modeled in basic KAPPA.

The prefilter is intended to function essentially as an interpolator/extrapolator of input data. An α-β filter of the basic form

$$\bar{X}_n = X_{pn} + \alpha(X_n - X_{pn})$$

$$\dot{\bar{X}}_n = \dot{\bar{X}}_{n-1} + \frac{\beta}{\Delta t}(X_n - X_{pn})$$

$$X_{pn} = \bar{X}_{n-1} + \Delta t\, \dot{\bar{X}}_{n-1} \quad ,$$

where $\bar{X}_n$ is a smoothed value of any variable at "n" and X_n is a data value of any variable at "n," was chosen for the simplicity provided by its sequential nature. It should be noted that in the present context, the state vector is defined as

$$X_n = \begin{bmatrix} R_n \\ AZ_n \\ EL_n \end{bmatrix}$$

as opposed to that discussed in the preceding section, although the subscript continues to represent a discrete time index ("pn" denotes a prediction at time n from the n-1th output). The values of α and β determine the bandwidth, and for optimally chosen values (in the sense of minimizing the mean square error) the filter is essentially a Wiener filter. As described in ref. 6, the prefilter can be made adaptive in a manner similar to the optional adaptive feature provided for KAPPA.

The performance of this prefilter and its effect on the overall system were not treated in the study described in Sec. 4.1.2. Considering the significant lag that became evident with sample runs of KAPPA (to be discussed), it is difficult to see how a prefilter can improve performance. The additional lag introduced would only further degrade overall real-time performance.

The adaptive feature was proposed for KAPPA to improve the transient response in the presence of severe transients. Without the adaptive feature and for steady-state conditions, the gain matrix, H_n, becomes constant (i.e., a constant bandwidth filter is attained) and yields poorer performance in the presence of transients. The adaptive bandwidth algorithm proposed in ref. 6 is

$$Q_n = K_1 H_n (Y_n - MX_{n/n-1}) + K_2 Q_{n-1} \quad *$$

which is used to update Q_n, the "system noise" covariance matrix, at each filter iteration. The quantity $H_n(Y_n - MX_{n/n-1})$ is simply the residual computed by KAPPA (see Figure 4-2) and is a measure of the deviation of the new observation from the predicted observable state variable estimates. K_1 and K_2 are constants to be determined. The rationale underlying the use of the algorithm is to use the quantity $H_n(Y_n - MX_{n/n-1})$ to detect radical departures from steady-state suspected to be transients in the state variables and to adjust the value of Q_n accordingly. In NASA-Wallops initial implementation, Q_n was always lower-limited to prevent it from becoming zero. (It is to be remembered that Q_n is involved in the computation of gain H_n.)

The adaptive feature was treated during this study but only for level flight representing essentially steady-state conditions and thus is not a

*It should be noted that this is a mixed expression in that the residual term is a vector and the Q terms are matrices (for K_1 and K_2 scalar).

complete test of its capability. The major concern of this formulation for making the filter adapt to transients is that filter convergence is not guaranteed. Other studies (ref. 7) have shown that a moving variance computation may be a more logical basis for transient detection. In the case of KAPPA, however, the computation load for calculating a moving variance could be prohibitive.

The optional feature for determining the effects of unmodeled parameters in KAPPA is an algorithm for estimating the error $S_{n/n}$ in the state covariance matrix $S_{n/n}$. In the derivation, the observation model given by equation (4-2) is modified to include an additive term so that

$$Y_n = M_n X_n + V_n + K_n \gamma_n$$

where γ is the vector of the unknown parameters not modeled in basic KAPPA, and K_n is a matrix of partial derivatives of the measurements with respect to the unmodeled parameters. The result of the derivation is a covariance error matrix

$$\Delta S_{n/n} = P_n \text{ Var } \gamma P_n^T$$

where

$$P_n = (I - H_n M_n) \Phi_n P_{n-1} - H_n K_n$$

is essentially a coordinate transformation, and Var γ represents the variances of the effective errors in range, azimuth, and elevation due to unmodeled parameters. Ref. 6 gives an example for computing the error due to radar biases, although the error due to any unknown parameter could be computed so long as it can be treated as an additive term. Investigation of this feature was not a part of this study.

4.1.2 KAPPA Simulation

To investigate the suitability of KAPPA for NASA LRC flight projects, a study was undertaken to exercise KAPPA in a manner similar to that in which it will be required to operate for providing needed data to flight research projects. A simulation was developed to represent an aircraft in flight with filtered data from KAPPA to be supplied as inputs to an on-board system. The CH-46 helicopter was chosen as the aircraft for several reasons:

1) the dynamic description of the CH-46 was one of the most conveniently available; 2) the aircraft flight control loop readily lends itself to simulation; and 3) the simulation of the particular system and flight conditions are realistic in terms of what would be expected of KAPPA operation in the runway facility.

A hybrid simulation was developed whereby the aircraft flight was simulated on an EAI 380 analog computer and the radar and KAPPA on a PDP-8 digital computer. Radar noise was simulated by a digital computer routine, and wind gusts on the aircraft were simulated with a low bandwidth, programmable noise generator (Hewlett-Packard Model 3722A).

To avoid unnecessary complexity, the helicopter simulation was limited to single-axis control, the vertical axis. The control loop equations and characteristics were obtained from ref. 8.* A diagram of the control loop simulated is given in Fig. 4-3. Note that provision is made for wind gusts.

The flight director network represents a VTOL flight director computer and display being researched at NASA LRC with the CH-46 helicopter. The inclusion of the flight director actually simplified the simulation since pilot functions were reduced to simple position following of the flight director computer commands. Note that altitude position, z, and altitude rate, $\dot{z}$, are required as inputs. It is required in the research project that instrumentation supply those data and it is thus reasonable to expect that supplying these inputs is a realistic demand of the runway facility and of KAPPA if it is to be used in the runway facility. KAPPA must therefore operate directly in the control loop. In this role, KAPPA's dynamic characteristics of gain, time lag, phase lag, and bandwidth are extremely important.

The overall guidance loop employed for simulation purposes is shown in Fig. 4-4. Note that the simulation provides the option of flying the helicopter with or without KAPPA in the feedback loop. Note also that even though helicopter dynamics were constrained to the z or vertical axis, horizontal position components x and y are also supplied to KAPPA.**

---

*Constraining the dynamics to a single axis permits a linear system description. Other investigators (ref. 8) indicate this constraint to closely approximate actual system behavior.

**It was initially hoped that a simplified version of KAPPA treating only z, $\dot{z}$, and $\ddot{z}$ as state vector components would be suitable for the simulation in order to reduce complexity. Comparison of results of this three-state variable version with results from the eight-state variable indicated considerable differences. The reason for the differences is due to the loss of cross-coupling among state variables in reducing the state vector dimensionality.

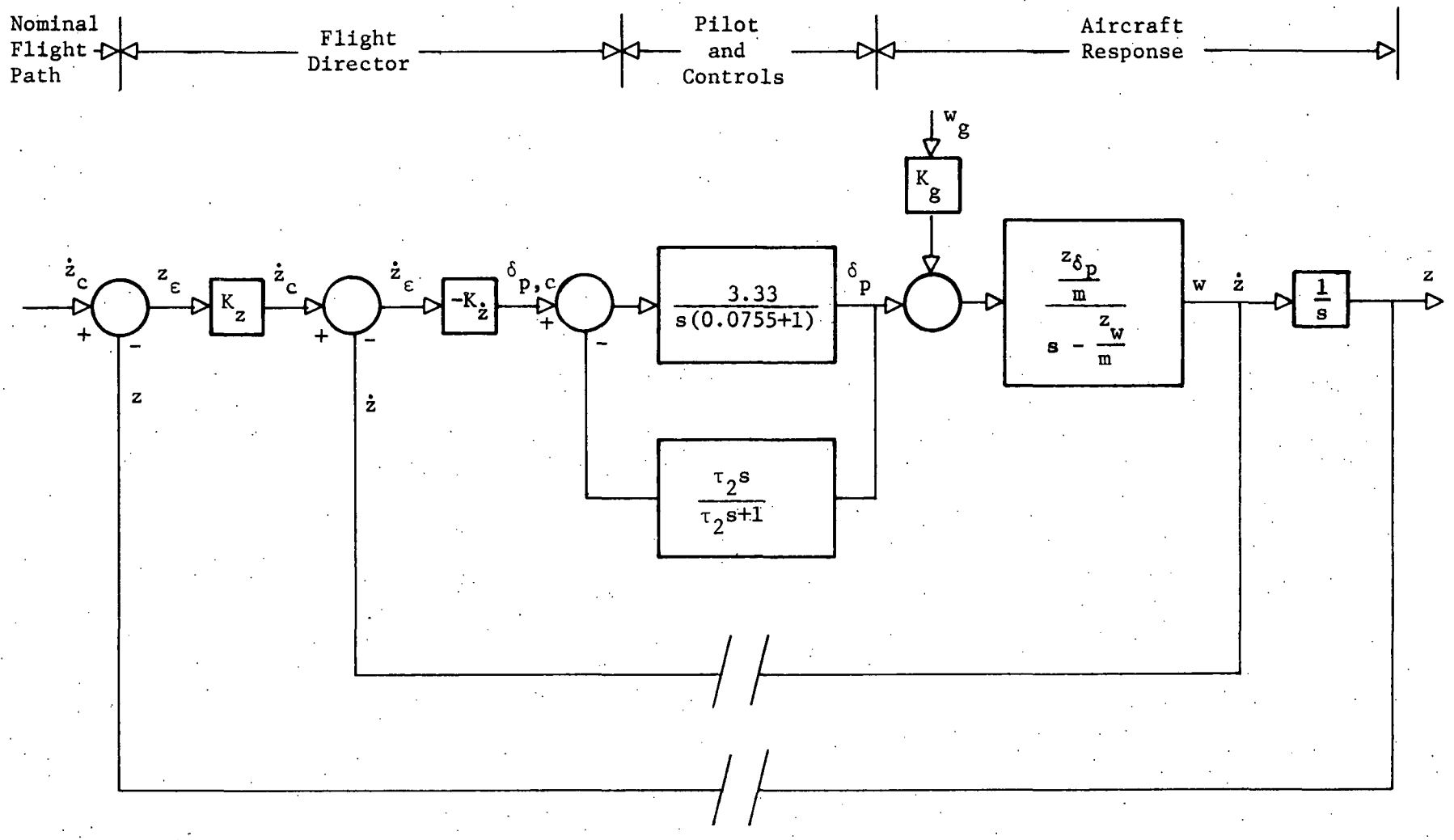

$K_z = 0.14$

$K_{\dot{z}} = 0.08$

$\tau_2 = 2.5$ sec

$K_g = \frac{z_w}{z_{\delta_p}} = 0.0621$

$\frac{z_{\delta_p}}{m} = -6.44$

$\frac{z_w}{m} = -0.4 \text{ sec}^{-1}$

Fig. 4-3. Helicopter vertical control dynamics.

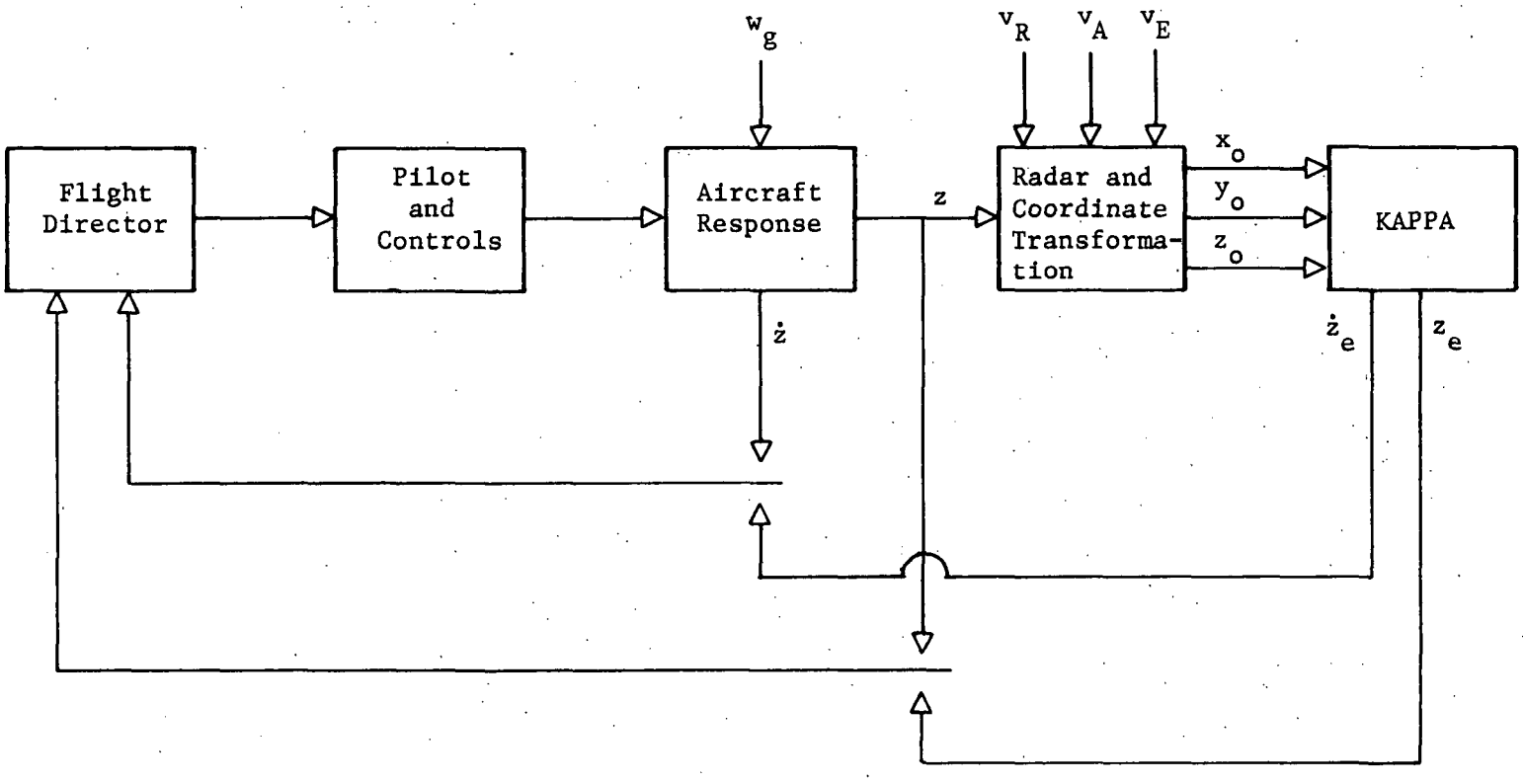

Fig. 4-4. Simulation loop of helicopter, radar, and KAPPA.

Inputs supplied to KAPPA in the simulation are

$$x_0 = x_n + v_x$$

$$y_0 = v_y$$

$$z_0 = z + v_z$$

where v_x, v_y, and v_z are radar noises. In these equations, flight is nominally constrained to the x-z plane with x_n representing the nominal value of x as programmed for a particular nominal flight path, and z representing the actual vertical position of the aircraft as it attempts to fly a nominally prescribed altitude z_n, typically programmed as a function of x. (For flight at small elevation angles and zero azimuth, the noises are adequately represented by $v_x = v_R$; $v_y = x_n \cdot v_A$; $v_z = x_n \cdot v_E$, where v_R, v_A, and v_E are radar range, azimuth, and elevation noise.)

All simulation runs were conducted with radar noise of 5 ft rms in range and 0.1 mil in azimuth and elevation. Figure 4-5 shows ten-second samples of this noise when converted to x, y, z coordinates.

Initial runs with basic KAPPA were conducted with a fixed Q matrix (i.e., fixed values of the diagonal elements in the range 0.1 to 10, which was the range of values that NASA Wallops had been obtaining with the optional adaptive feature with representative tracking data used for testing the filter). In the helicopter simulation runs with basic KAPPA, using these Q values resulted in excessive smoothing, thus erasing aircraft maneuver in the output data. An investigation was undertaken to determine the appropriate order of magnitude of Q's.

Given a system model as in Fig. 4-3 with a prior knowledge of disturbances, it is theoretically possible to derive the true Q to use in the filter. This requires, however, converting the covariances of the system disturbance for the analog model to an equivalent set for the discrete form of the model as is assumed for filter formulation.

The general continuous-time system model is given by

$$\dot{X}(t) = F(t)\, X(t) + G(t)\, W(t)$$

where X(t) is the state vector, W(t) is the disturbance input vector, and

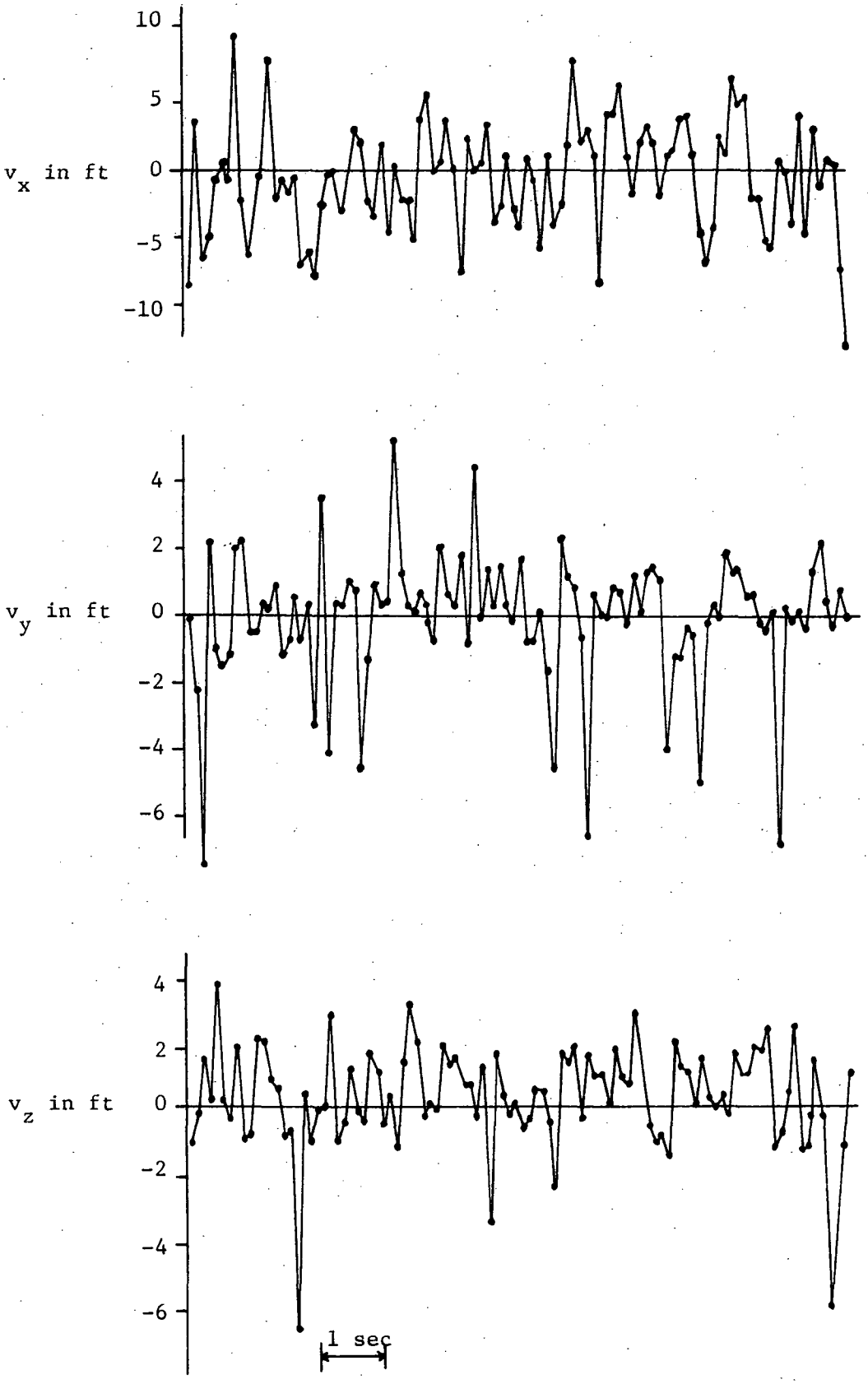

Fig. 4-5. Samples of radar noise used in the simulation.

F(t) and G(t) are system matrices governing the system response to these inputs. This is the analog counterpart of the discrete-time model

$$X_k = \Phi_k X_{k-1} + \Gamma_k W_k$$

presented earlier. From known characteristics of G(t) and W(t), $\Gamma_k W_k$ can be identified and used to specify the Q matrix.

It is shown in ref. 9 that in going from the continuous to the discrete representation, the following relationships are obtained:

$$\Phi(t + \Delta t, t) \simeq I + F(t)\,\Delta t \tag{4-7}$$

and

$$\Gamma(t + \Delta t, t) \simeq G(t)\,\Delta t \quad . \tag{4-8}$$

Consider now the aircraft response portion of the loop in Fig. 4-3. The transfer functions given are equivalent to

$$z = \frac{d\dot{z}}{dt} = \frac{z_w}{m}(z + w_g) + \frac{z_{\delta_p}}{m}\delta_p$$

and

$$z = \frac{dz}{dt} \quad .$$

Considering only the response to the w_g input (i.e., $\delta_p = 0$) and letting $x_1 = z$, and $x_2 = \dot{z}$ be the logical choice of state variables,

$$\dot{x}_1 = x_2$$

$$x_2 = \frac{z_w}{m} x_2 + \frac{z_w}{m} w_g$$

which in state space matrix form is

$$\begin{bmatrix} \dot{x}_1 \\ \dot{x}_2 \end{bmatrix} = \begin{bmatrix} 0 & 1 \\ 0 & \frac{z_w}{m} \end{bmatrix} \begin{bmatrix} x_1 \\ x_2 \end{bmatrix} + \begin{bmatrix} 0 & 0 \\ 0 & \frac{z_w}{m} \end{bmatrix} \begin{bmatrix} w_1 \\ w_2 \end{bmatrix} \quad . \tag{4-9}$$

Comparing eq. (4-9) with eq. (4-6) shows that

$$F(t) = \begin{bmatrix} 0 & 1 \\ 0 & \frac{z_w}{m} \end{bmatrix} \quad \text{and} \quad G(t) = \begin{bmatrix} 0 & 0 \\ 0 & \frac{z_w}{m} \end{bmatrix}$$

Substituting into eqs. (4-7) and (4-8) yields

$$\Phi_k = \begin{bmatrix} 1 & \Delta t \\ 0 & 1 + \frac{z_w}{m} \Delta t \end{bmatrix}$$

and

$$\Gamma_k = \begin{bmatrix} 0 & 0 \\ 0 & \frac{z_w}{m} \Delta t \end{bmatrix}$$

Therefore

$$\Gamma_k W_k = \begin{bmatrix} 0 \\ \frac{z_w}{m} \Delta t \; w_{g_k} \end{bmatrix}$$

from which it is easily shown that

$$Q_{discrete} = E\{\Gamma_k W_k \cdot (\Gamma_k W_k)^T\} = \begin{bmatrix} 0 & 0 \\ 0 & (\frac{z_w}{m})^2 (\Delta t)^2 E\{W_{g_k}^2\} \end{bmatrix} = \begin{bmatrix} 0 & 0 \\ 0 & (\frac{z_w}{m})^2 \Delta t^2 Q_{continuous} \end{bmatrix} \tag{4-10}$$

Unless otherwise specified, wind gust noise used in all runs was gaussian white noise bandlimited to 1.5 Hz (10 rad/sec) with zero mean and an rms of 2 ft. A sample of this noise is shown in Fig. 4-6. Therefore, using $\frac{z_w}{m} = -0.4 \text{ sec}^{-1}$ and $\Delta t = 0.1$ sec,

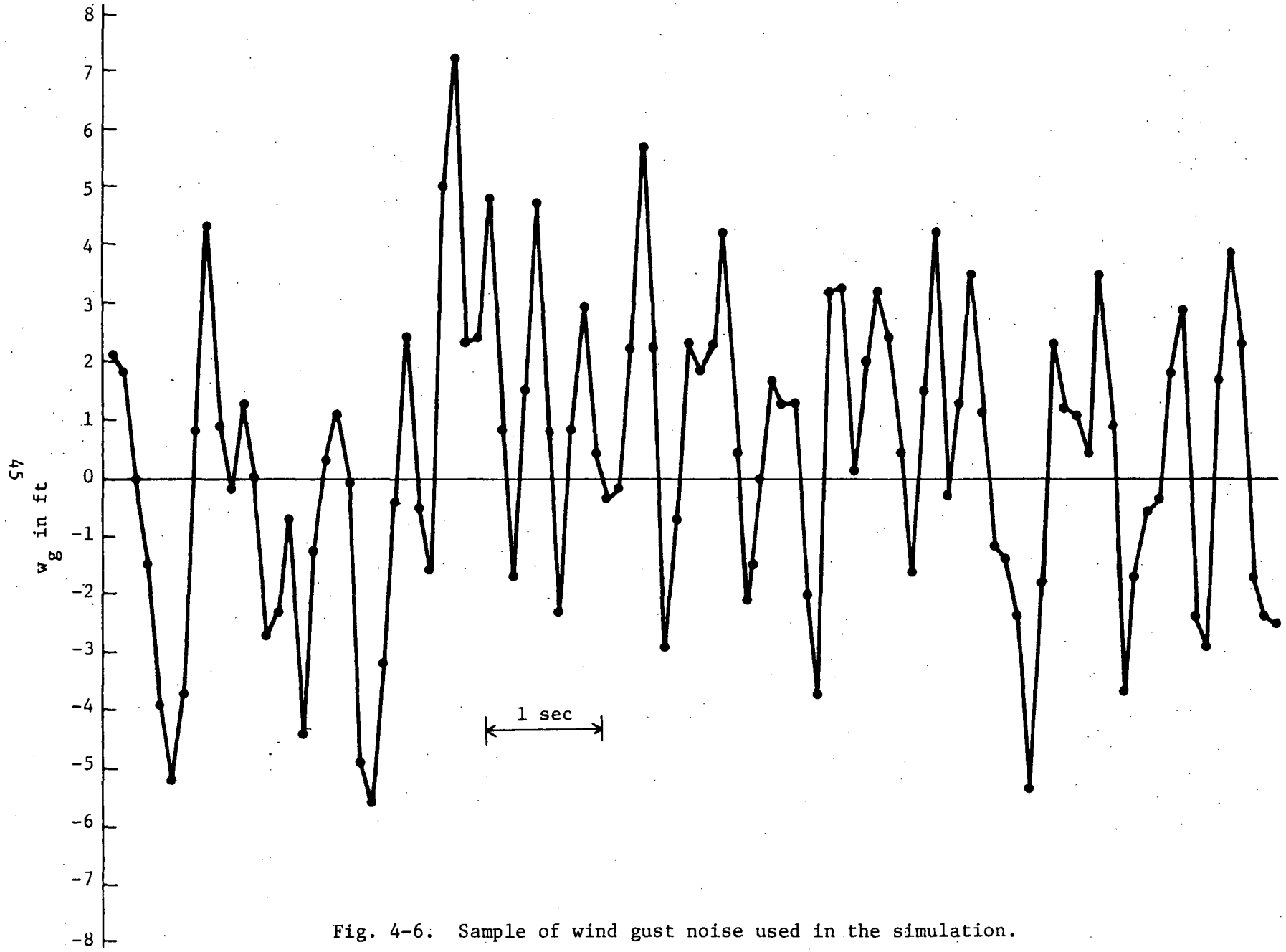

Fig. 4-6. Sample of wind gust noise used in the simulation.

$$q_{22} = \left(\frac{z_w}{m}\right)^2 (\Delta t)^2 Q_{continuous} = 0.0064 \quad (ft/sec)^2$$

as the value in equation (4-10). Note that this term is associated directly with $\dot{z}$, the azimuth rate, and would thus represent the true value for q_{66} for the KAPPA Q-matrix. Furthermore, since this is the only system noise in the simulation, all other Q-values are theoretically zero. It has been demonstrated by NASA Wallops, however, that when diagonal Q elements are set to zero, KAPPA appears to lower its bandwidth and provides excessive smoothing. For this reason, all filter runs were made with finite values of all diagonal elements of the Q-matrix.

Figures 4-7 and 4-8 demonstrate the performance of KAPPA with $q_{66} = 0.0064$ and all other diagonal elements set at 0.001.* For this run, the helicopter was started on a level flight and allowed to respond only to wind gusts, i.e., δ_p as shown in Figure 4-3 was constrained to zero, which makes this run compatible with the Q conditions derived above. Here, z and $\dot{z}$, shown in Figures 4-7 and 4-8, represent signals for filtering purposes to be recovered. z_o represents the signal-plus-noise from which z_e and $\dot{z}_e$ are to be estimates; however, recall that the filter also has x_o and y_o inputs which include radar noise.

Figures 4-7 and 4-8 show relatively good estimates of z and $\dot{z}$ but with considerable lag (on the order of 1.5 to 2 sec) in the outputs. To investigate the accuracy of the derived Q value of 0.0064 for q_{66}, additional runs were made with q_{66} varied an order of magnitude above and below the derived optimum value. Results are shown in Figures 4-9 and 4-10.

Referring first to the rate estimates in Figure 4-10, the filter with $q_{66} = 0.00064$ obviously provides excessive smoothing. True variance calculations were not done concurrently with the estimation. Judgment is thus based on appearances in the graph. In comparing the estimates for $q_{66} = 0.064$ and 0.0064, the larger value appears to provide slightly better accuracy; however, it is considerably noisier than the lower value. The estimate for $q_{66} = 0.0064$ appears more representative of what one would expect from an acceptable filter.

The estimates of position shown in Figure 4-9 tend to substantiate the preference of $q_{66} = 0.0064$ over the higher and lower values. The trace is less noisy than the higher value and has less overshoot.**

---

*The initial portion of the estimates (approximately the first two sec) in these and all later plots include start-up transients.

**Results of other runs not shown also showed considerable overshoot for the higher value of q_{66}.

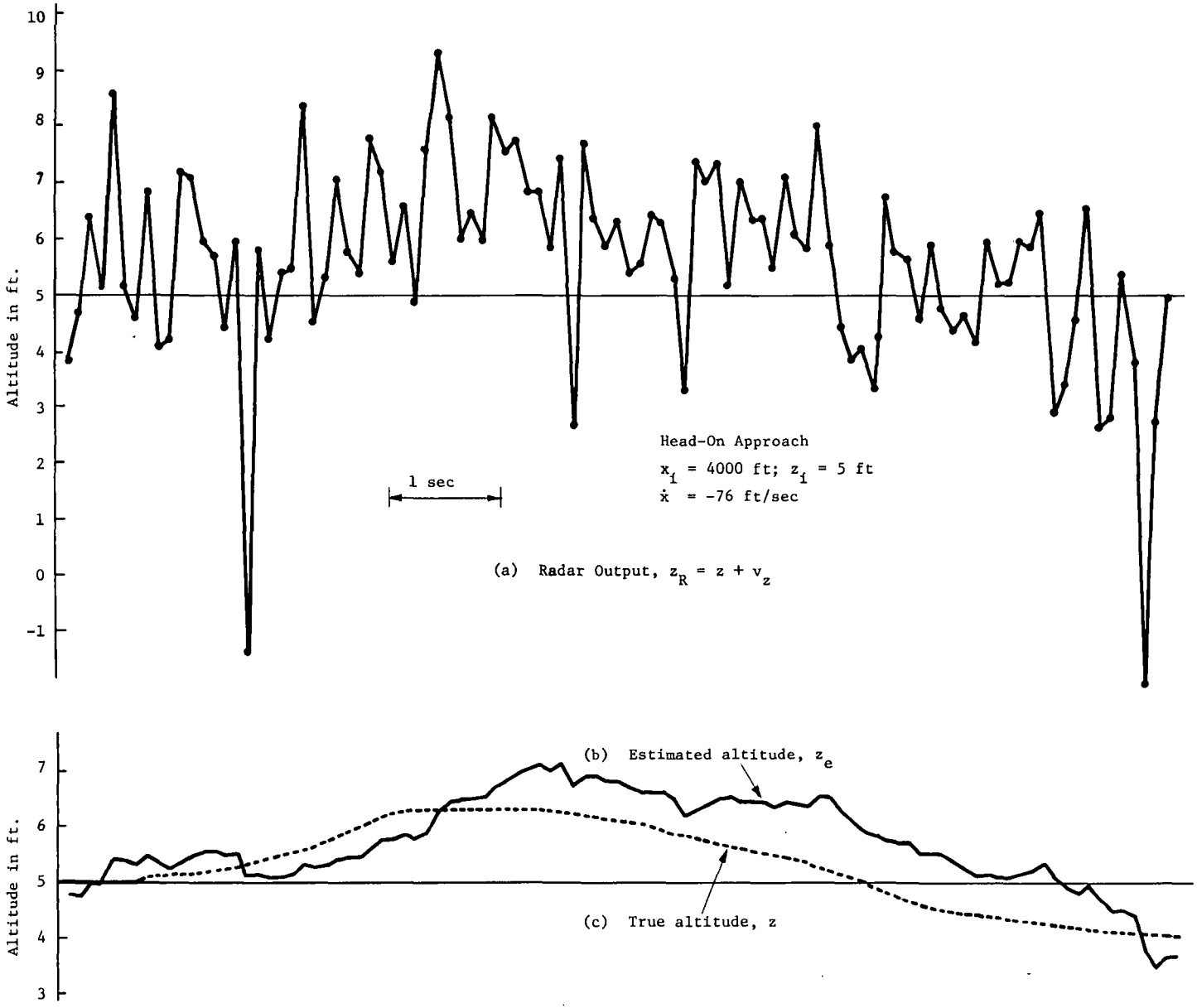

Fig. 4-7. Altitude estimation with KAPPA.

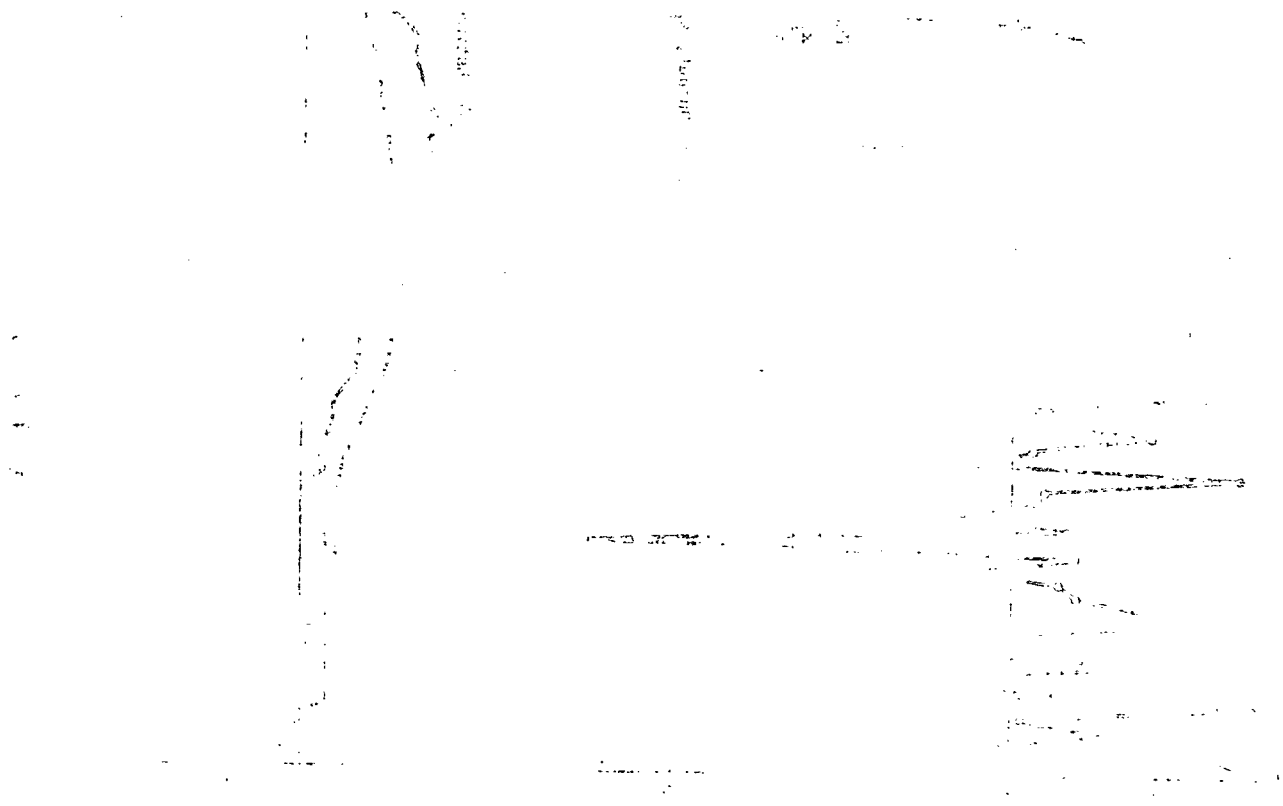

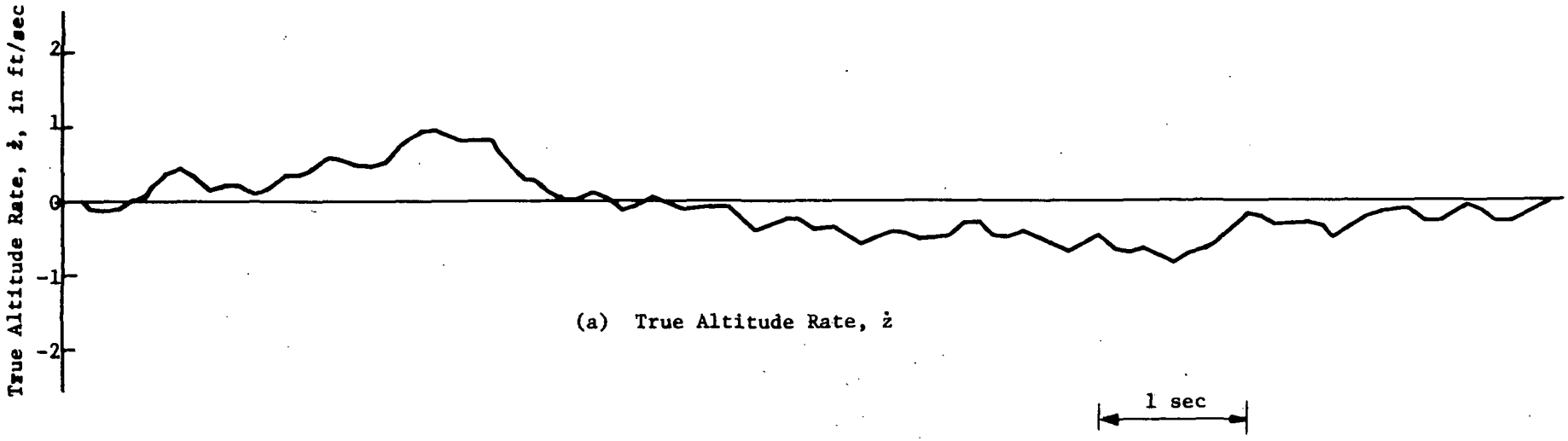

(a) True Altitude Rate, $\dot{z}$

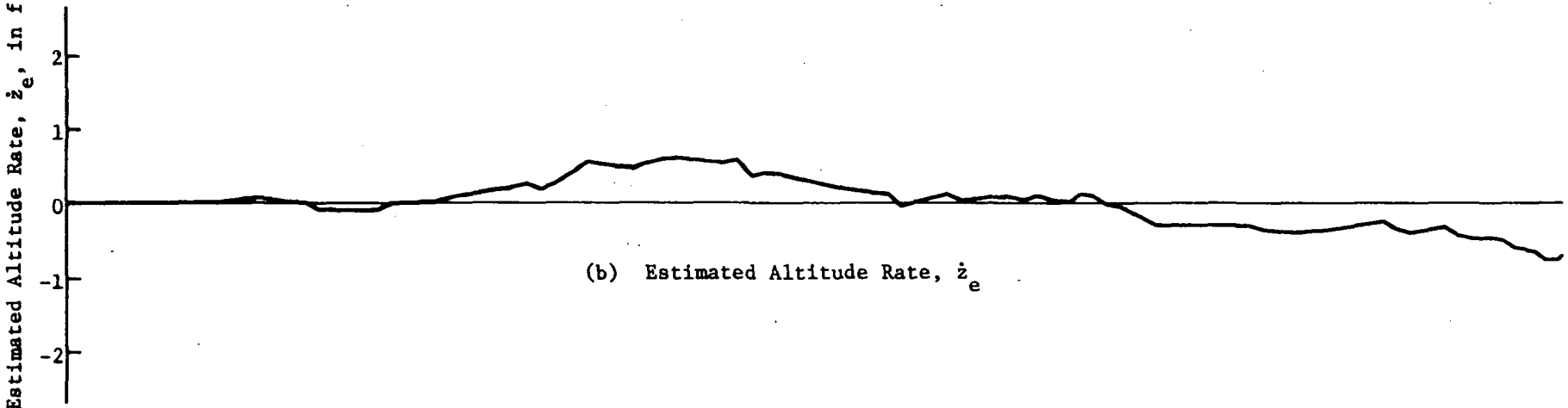

(b) Estimated Altitude Rate, $\dot{z}_e$

Fig. 4-8. Rate estimation with KAPPA.

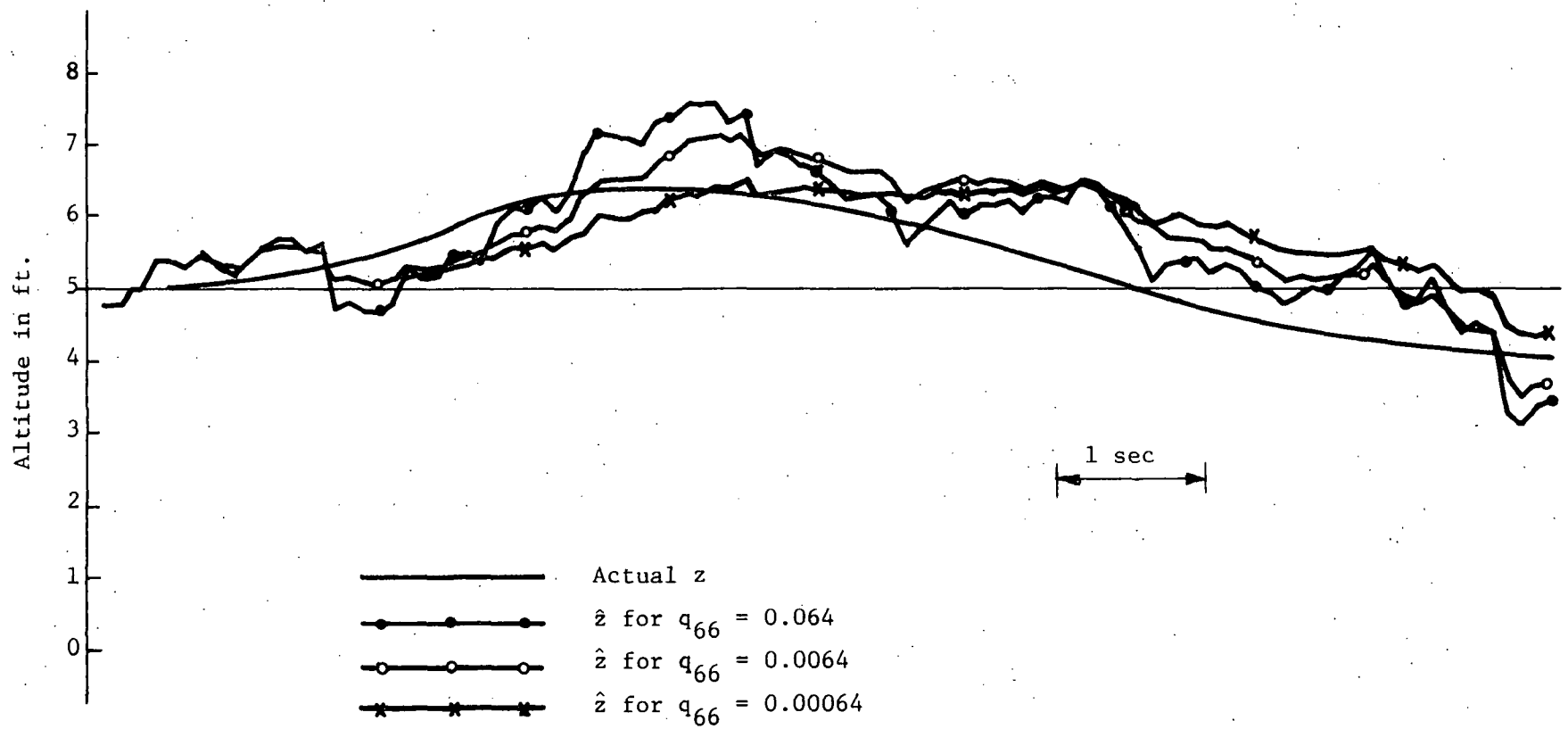

Fig. 4-9. Comparison of actual and estimated values of z versus time for various values of q (CH-46 helicopter-aerodynamic loop only as system model).

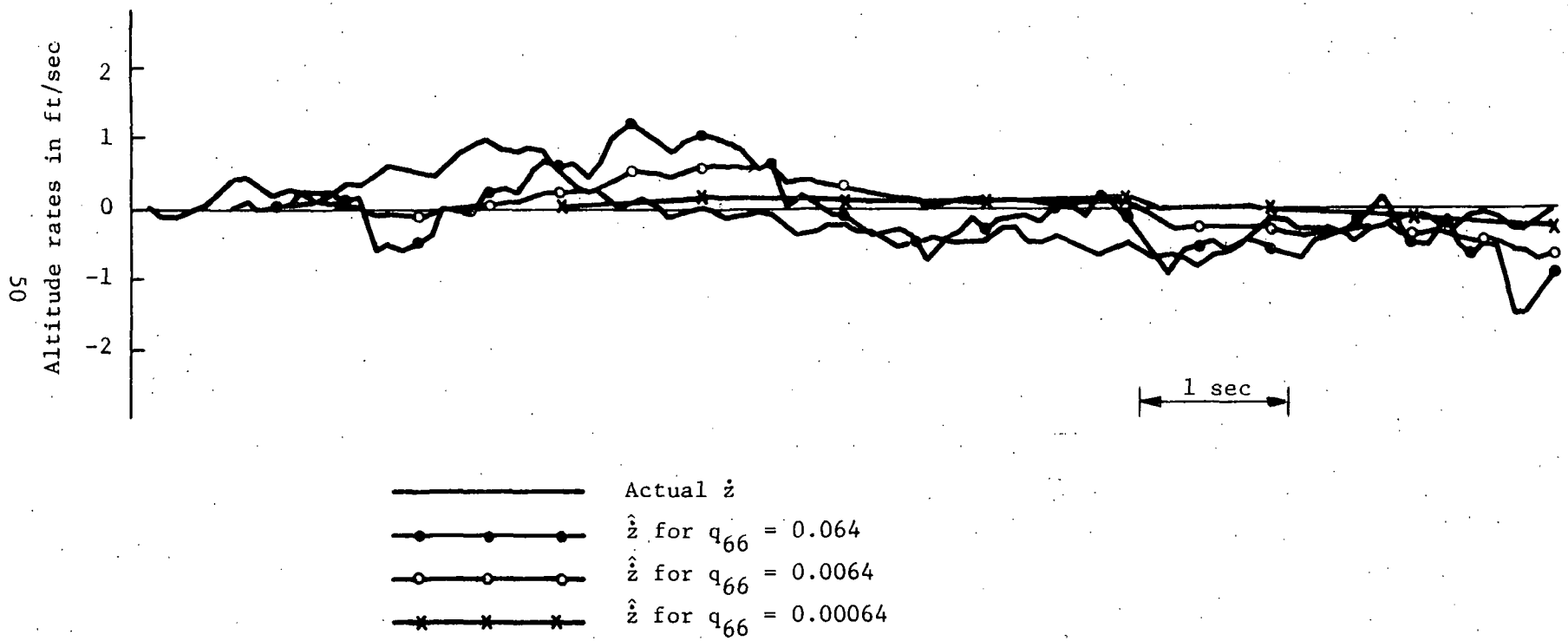

Fig. 4-10. Comparison of actual and estimated values of z versus time for various values of q (CH-46 helicopter-aerodynamic loop only as system model).

It is recalled that the above results are for only the aerodynamic loop of the aircraft serving as the system model. Attempts to use the full aircraft control loop description (Figure 4-3) as the system model in the derivation of optimum Q values leads to an unwieldy solution. (Specifically, the Q elements q_{33} and q_{66} are functions of derivatives of w_g.) Recognizing that the bandwidth of the aerodynamic loop is about the same as the bandwidth of the total control loop, it is reasonable to expect that the same Q values are nominally the actual values needed. Figures 4-11 and 4-12 show results of simulation runs for the total loop under the same conditions as those for the aerodynamic loop only with results given in Figures 4-9 and 4-10. (In comparing Figures 4-11 and 4-12 with Figures 4-9 and 4-10, the reader should be aware of a difference in scale on the ordinates.) For these runs, the aircraft control loop was closed on the analog computer and not through the simulated radar and KAPPA, and the actual response curves thus represent the behavior that would be obtained with perfect z and $\dot{z}$ sensors.

The filter behaviors as characterized by the estimates are similar to those shown earlier displaying similar lag and variation with q_{66}.

As noted in earlier discussion, a required role for KAPPA in the CH-46 program would be to supply the position and rate data required as input to the flight director being studied, and in this role KAPPA would have to operate as an element in the overall aircraft control loop. Simulation runs were conducted to investigate KAPPA's ability in this regard. A typical response for an extended period of time is shown in Figures 4-13 and 4-14. With KAPPA in the loop, the loop appears in places to be on the verge of instability, as characterized by the apparent overshoot and subsequent "ringing." Some of this effect can obviously be attributed to the lag noted earlier that results from KAPPA. It is emphasized that all of the lag in this case is phase lag. In the simulation, the sampling and computation with KAPPA were done at each iteration with the analog computer in the HOLD mode (i.e., z and $\dot{z}$ were estimated and fed back prior to the next iteration). With the large magnitude (up to 2 sec) of phase lag observed, the time lags expected (0.1 to 0.2 sec) in the runway facility should have little additional effect.

A considerable part of the undesirable loop behavior occurring with KAPPA in the loop (as in Figure 4-13) could readily result from position overshoot obtained solely from KAPPA, which was recognized earlier (and as is evident in Figure 4-9, for example) and which, in effect, is an additional

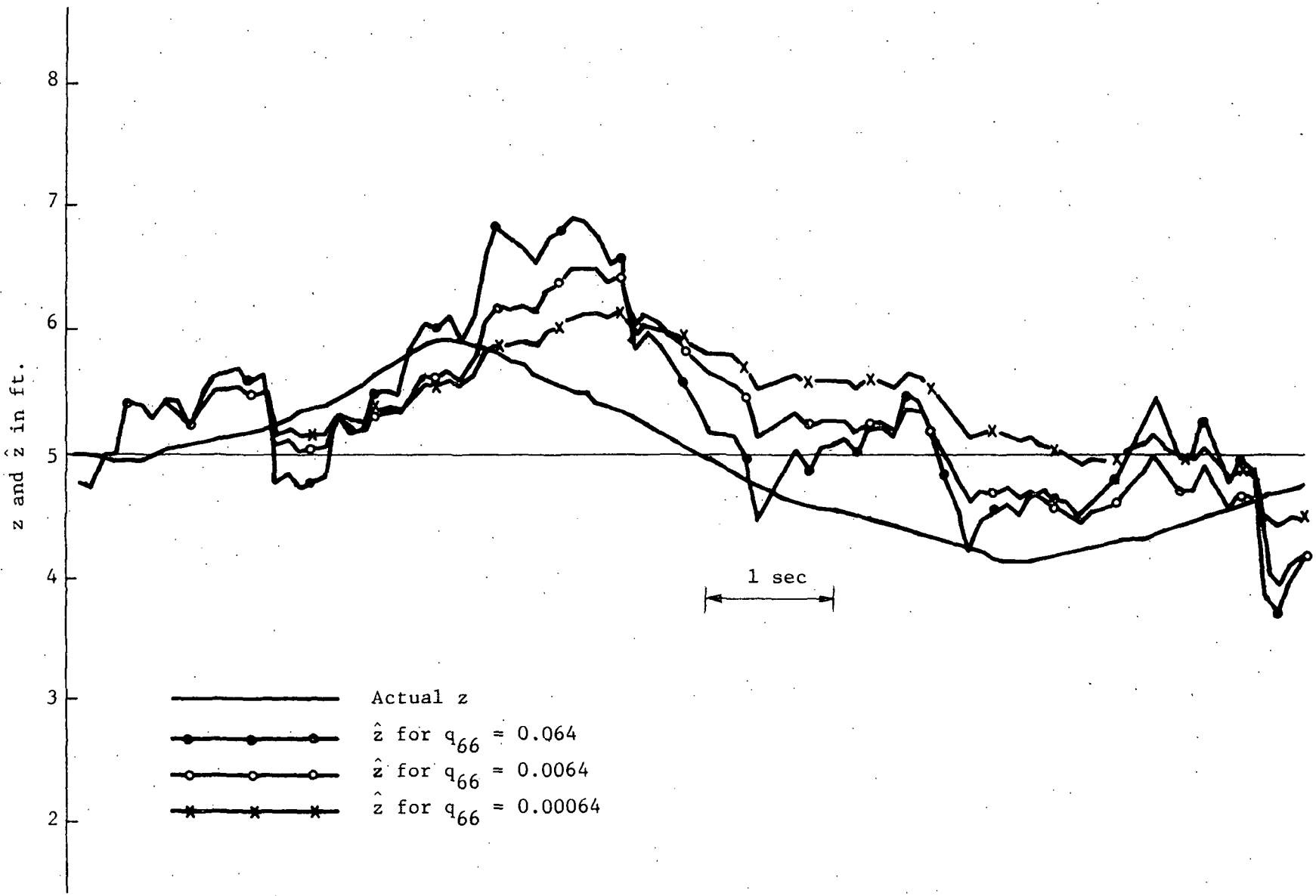

Fig. 4-11. Comparison of actual and estimated values of z versus time for various values of q (CH-46 helicopter-perfect z and ż observations).

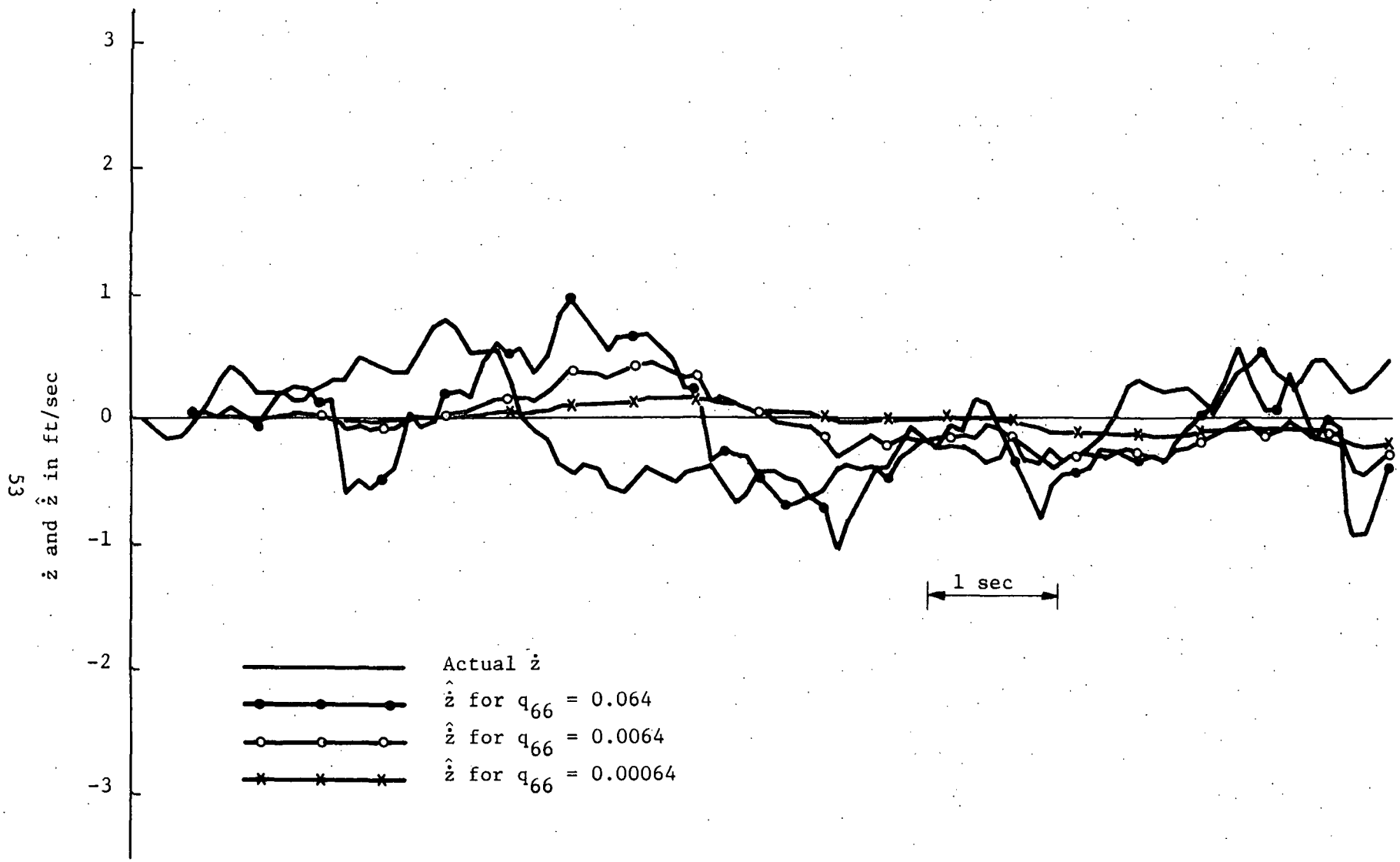

Fig. 4-12. Comparison of actual and estimated values of ż versus time for various values of q (CH-46 helicopter-perfect z and ż observation).

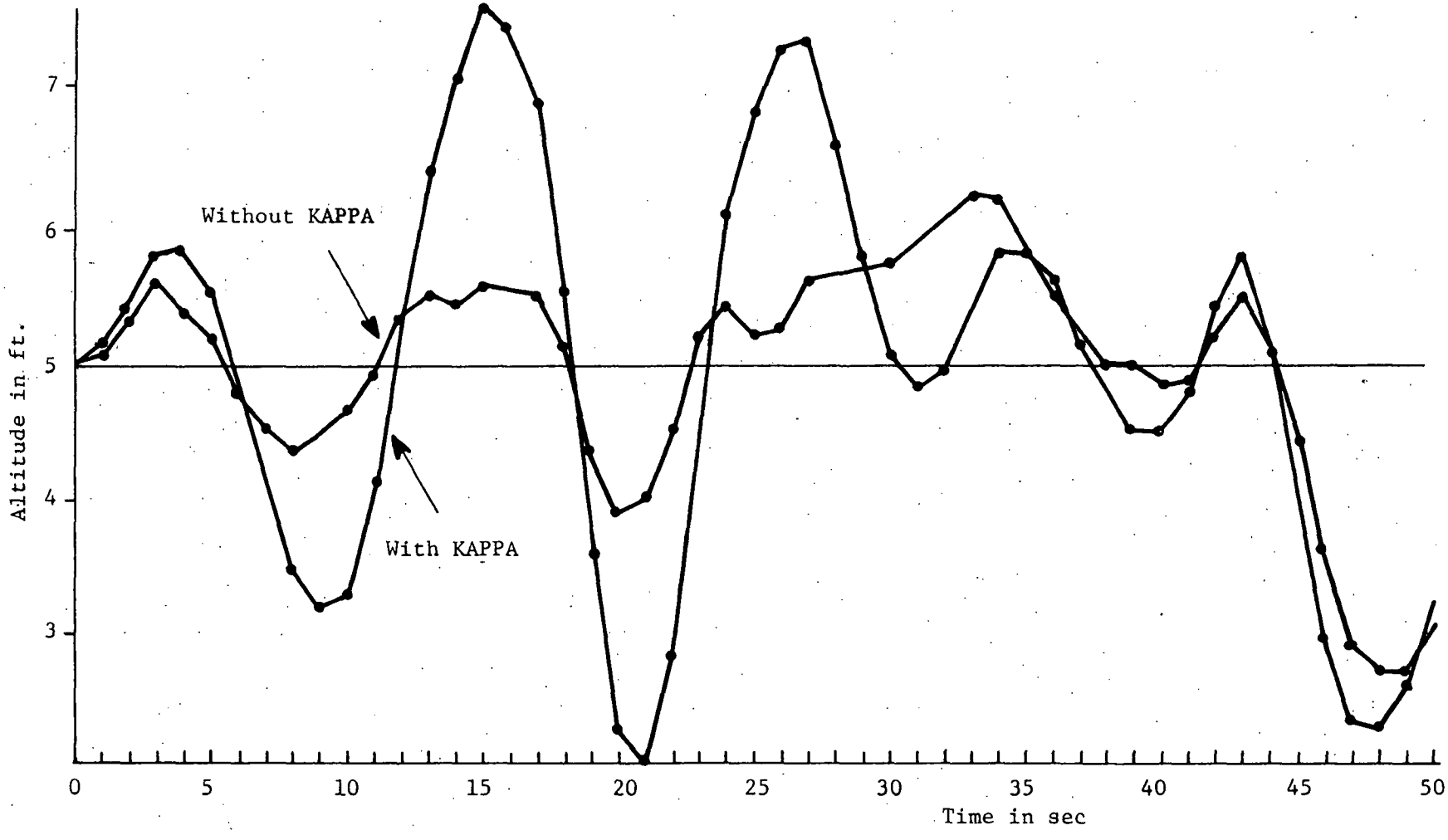

Fig. 4-13. Comparison of the helicopter altitude response with and without KAPPA in the control loop.

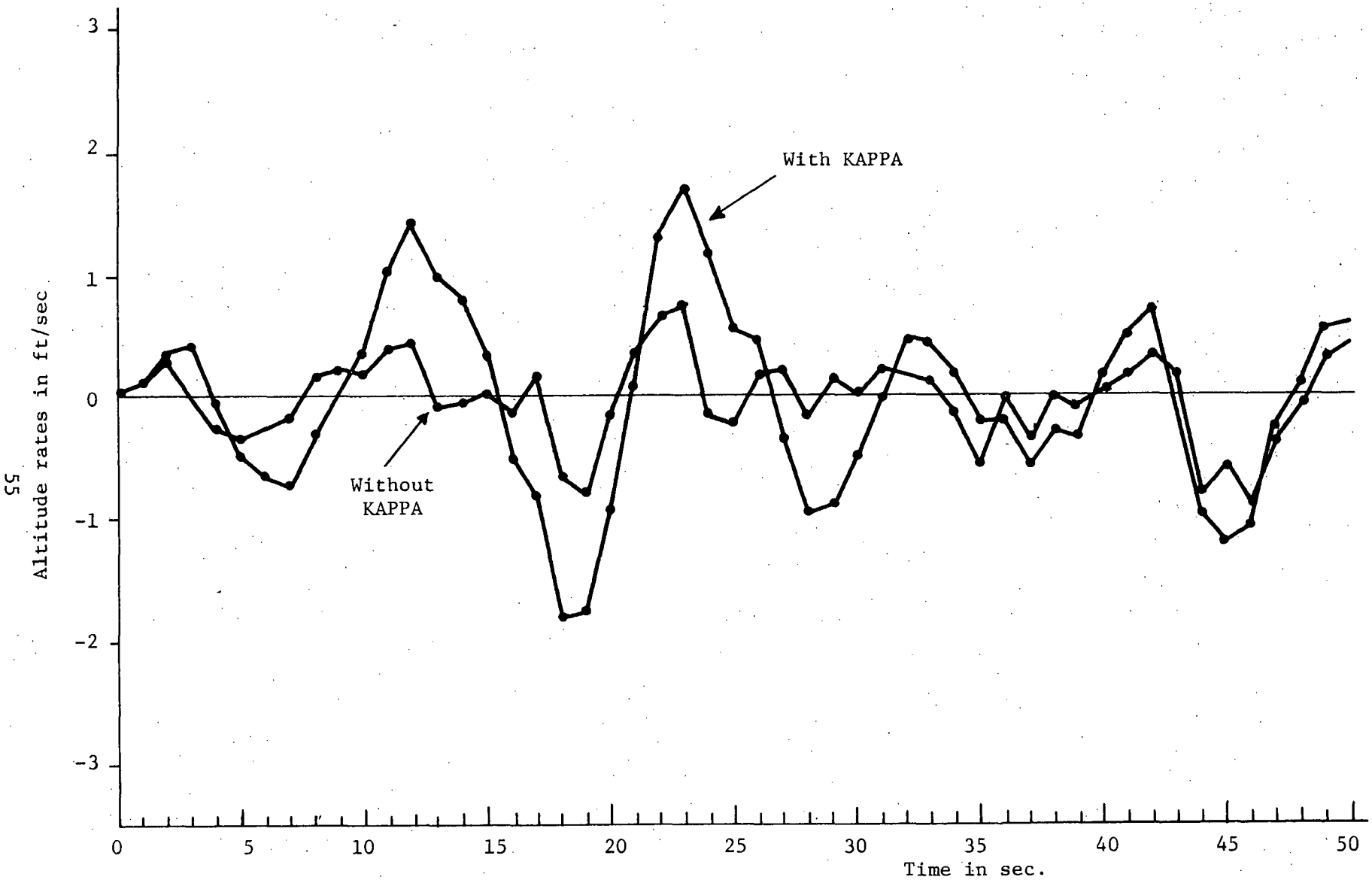

Fig. 4-14. Comparison of altitude rate response of the helicopter with and without KAPPA in the control loop.

gain in the loop, causing the loop to behave accordingly. This is not, in the strict sense, a fault of KAPPA, since the overshoot can depend on the choice of the Q-values used. This is not an altogether unreal situation, however, since in actual operation in the runway facility the true Q-values will never be known. The best guesses of Q's, whether for system (aircraft) disturbances or for the unmodeled parameters (Section 4.1.1.2), could potentially cause similar behavior.

It should be noted that all of the above results are based on fixed Q-values throughout each run. The adaptive Q version of KAPPA described in Section 4.1.1.2 was proposed in ref. 6 as a way of making KAPPA more responsive to large transients. Several runs were conducted with the adaptive feature included in the simulation described. These were all under level flight (and therefore essentially steady-state) conditions and little change in the response over those presented earlier was noticed. The adaptive feature offered no reduction in the lag observed. This is because the adaptive feature was actually intended to aid the response for considerably larger transients than those occurring in the flight conditions simulated.

Simulation runs under more severe transient conditions as might be encountered during approach and landing were not included as a part of this study. NASA Wallops is conducting studies to assess real-time performance of KAPPA, and these studies will include the investigation of the adaptive Q feature.

Based on the investigations to date, it appears that KAPPA has limited potential for use in the runway facility, especially for real-time applications in which it will be required to operate as an element in a closed guidance loop. Whereas the dynamic characteristics (gain and phase lag) may be no worse (and even better in some cases) than alternate filters, the fact that these characteristics will be constantly changing and will not be accurately known will be a disadvantage to its use in this regard. The greatest use of KAPPA will most likely be in an open loop mode to serve as a post-flight data smoother or, in real-time, to supply plotters and recording devices. For any use of KAPPA in a closed-loop system, whether for simple ILS signal generation or for complex inputs to control systems, careful consideration should be given by each user to determine the effect of filter dynamics on test results. Any effort by NASA LRC in this regard should be closely coordinated with studies being performed by NASA Wallops.

4.2 Laser Eye Safety

Since a laser tracker is to be used in the runway facility, it is necessary from the standpoint of personnel safety to consider the potential hazards involved and to assure that proper safety measures are taken. The major concern in this tracking application of a laser is eye safety of the pilots, flight crews, ground crews, runway tower personnel, and any other persons within laser range.

This section reviews the eye safety problem with lasers and presents analyses of exposure levels of two laser types previously proposed for runway operation.

4.2.1 Eye Hazards

Much has appeared in the literature on the laser eye safety problem. Good tutorial descriptions are given by Ham, et al. (refs. 10, 11, and 12) and by van Pelt (ref. 13). Extensive experimentation (refs. 14 to 17) has been performed to measure damage thresholds as a basis for establishing permissible exposure levels.

Eye hazards with laser radiation depend on many factors, typical of which are:

(1) wavelength of radiation
(2) radiation intensity at the cornea
(3) background intensity and pupil size
(4) eye focus
(5) laser beamwidth
(6) spatial uniformity of the beam
(7) peak pulse power
(8) pulse width
(9) pulse spacing or prf
(10) average power
(11) exposure time.

The part of the eye most sensitive to radiation is the retina. The transmittance of the ocular media vs. wavelength is shown in Fig. 4-15, which illustrates the familiar spectral region of major concern for retinal damage to be the 0.4 to 1.4 μ wavelength portion. Even with the extensive investigations conducted to date, retinal damage mechanisms are not fully understood. Much is known to be due to heating effects; however, other effects such as shocks from radiation pressure, steam generation, ionization,

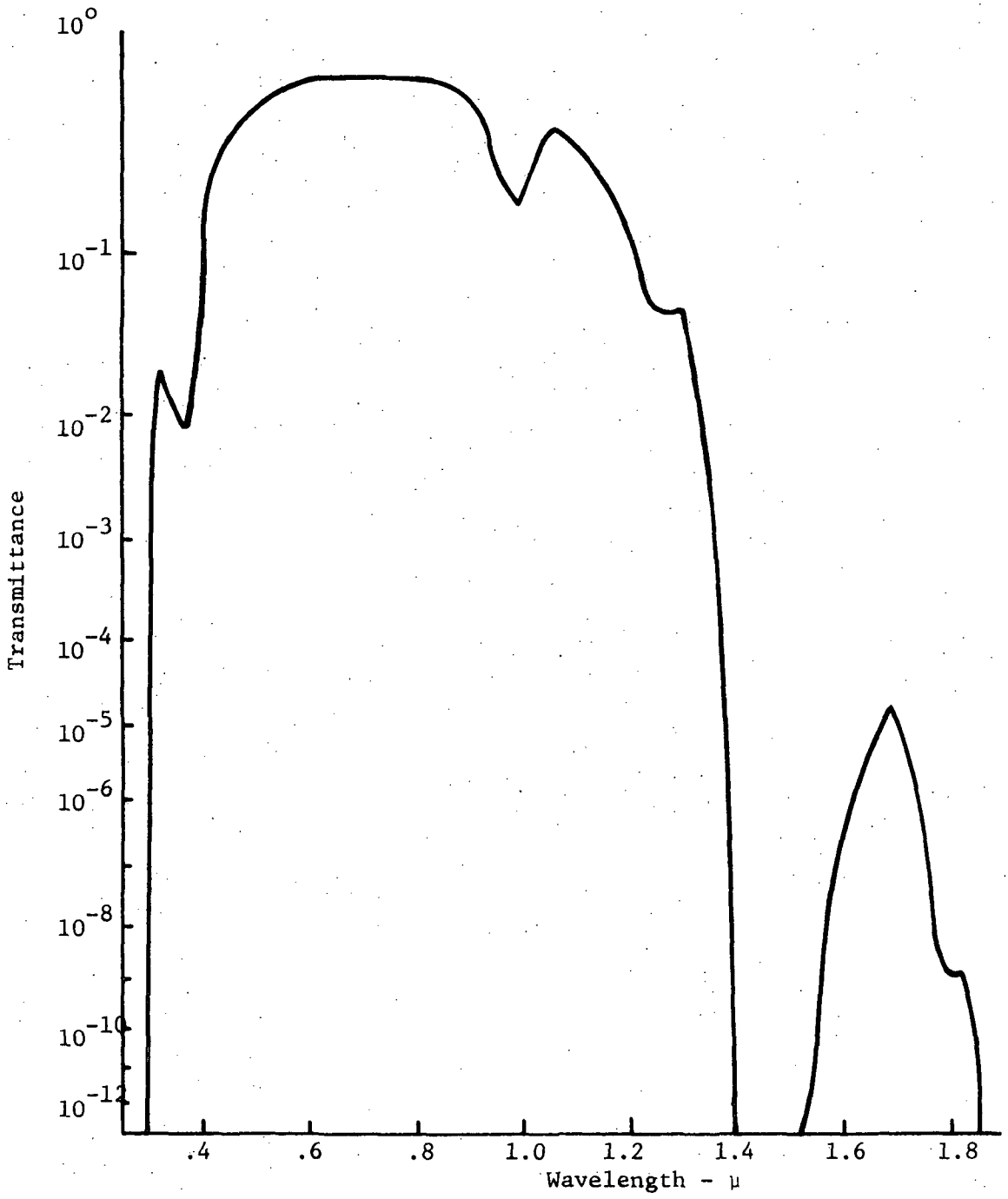

Fig. 4-15. Spectral transmittance through human eye. Between 0.3 and 1.3μ, the curve is based on measurement of human ocular tissues. Beyond 1.3μ the transmittance is that of 2.2 cm layer of pure H_2O.

and sonic transients, especially with short Q-switched pulses, are considered possible sources of damage (refs. 10, 11, and 18). At high exposure levels, for Q-switched pulses, retinal tissue can actually be expelled into the vitreous humor. Most experimentation to date has concentrated on measuring exposure thresholds for retinal damage, with damage usually defined as the smallest opthalmoscopically visible lesion on the retina. Many investigators believe that damage may be occurring at exposure levels below the threshold and may also be cumulative. Ham and Walkenbach (ref. 18) currently conducting experiments which will provide more knowledge on damage mechanisms and effects; results to date of this work are inconclusive.

Ultraviolet (UV) radiation at wavelengths below 0.4 μ is absorbed by the cornea and overexposure can cause a photophobic condition and painful inflammation known as keratitis. The action of UV radiation is thought to be photochemical rather than thermal (ref. 19) Exposure levels and durations for UV radiation required to produce damage are considerably greater than those for wavelengths damaging to the retina.

At wavelengths beyond 1.4 μ in the near and far infrared (IR) region, radiation is not a hazard to the retina. Prolonged or chronic exposure to radiation at these wavelengths, however, can cause overheating of the lens leading to opacification, a hazard known as infrared cataract and sometimes referred to as glassblowers' or steelpuddlers' cataract. The mechanism causing opacification of the lens is denaturation of the lens proteins. The effect is similar to that caused by overexposure to microwaves.

4.2.2 Standards and Regulations

Recognizing the hazards of laser radiation, many governmental, industrial, and private organizations have set standards for exposure to laser radiation. Because of lack of knowledge and agreement on the severity of the hazards, existing standards vary widely and are continually changing. The Army, Navy, and Air Force, sponsoring extensive research in measuring damage thresholds, have recently agreed (ref. 20) on maximum permissible exposure levels which are considerably more liberal than earlier ones specified by the Army and Navy (ref. 13) and by the American Conference of Governmental Industrial Hygienists (ref. 21). Standards are also evolving through the efforts of the now-famous Z-136 Committee of the American National Standards Institute (ANSI), which are more detailed than those specified by the military services. According to Wolbarsht (ref. 23), Head

of the Eye Hazards Subcommittee of the ANSI Z-136 Committee, MPE levels in the final version of the standards will probably be about the same as those in the tri-service standards. As authorized by the Health and Safety Act of 1968, the Bureau of Radiological Health is also undertaking efforts to establish regulations and to control laser radiation. It is expected that the ANSI and tri-service standards will be a major input to the Federal regulations.

For radiation in the spectral range from 0.4 μ to 0.694 μ, MPE levels specified in the latest ANSI standards (ref. 23) are as follows:

Exposure Time, t (sec)	Power Into Eye (watts)	MPE at Cornea (watt/cm^2)	Radiant Exposure (joule/cm^2)
2×10^{-5} to 10	$0.69 \times 10^{-3}\ t^{-1/4}$	$1.8 \times 10^{-3}\ t^{-1/4}$	$1.8 \times 10^{-3}\ t^{3/4}$
10^{-9} to 2×10^{-5}	$1.9 \times 10^{-7}\ t^{-1}$	$5.0 \times 10^{-7}\ t^{-1}$	5.0×10^{-7}
10 to 10^4			10^{-2}
$> 10^4$			10^{-6}

The conversion from "power into eye" to "MPE at cornea" is based on a pupil diameter of 7 mm and the eye focused at infinity. The values listed for exposure times greater than 10 sec are presented by ANSI as guidelines only, as there is a scarcity of data for these exposure times. A plot of the standards is given in Fig. 4-16.

Additionally, for longer wavelengths and pulse repetition rates greater than unity the MPR values are increased. Figs. 4-17 and 4-18 show plots of the correction factors associated with these increases (ref. 22).

4.2.3 Safety Measures

The possible existence of safety hazards with laser radiation is determined by computing the possible radiation intensities, via direct or reflected paths, and comparing them with the MPE levels established by standards. When the intensities exceed the MPE levels, safety measures must be considered. Typical safety measures are system redesign for safe levels, laser goggles, protective barriers, radiation cut-out zones, laser power programming, elimination of reflecting surfaces, safety interlocks, and warning or caution signs and symbols.

Laser safety goggles are now manufactured by several optical companies. Goggles are usually rated in terms of an optical density quantity, D, where

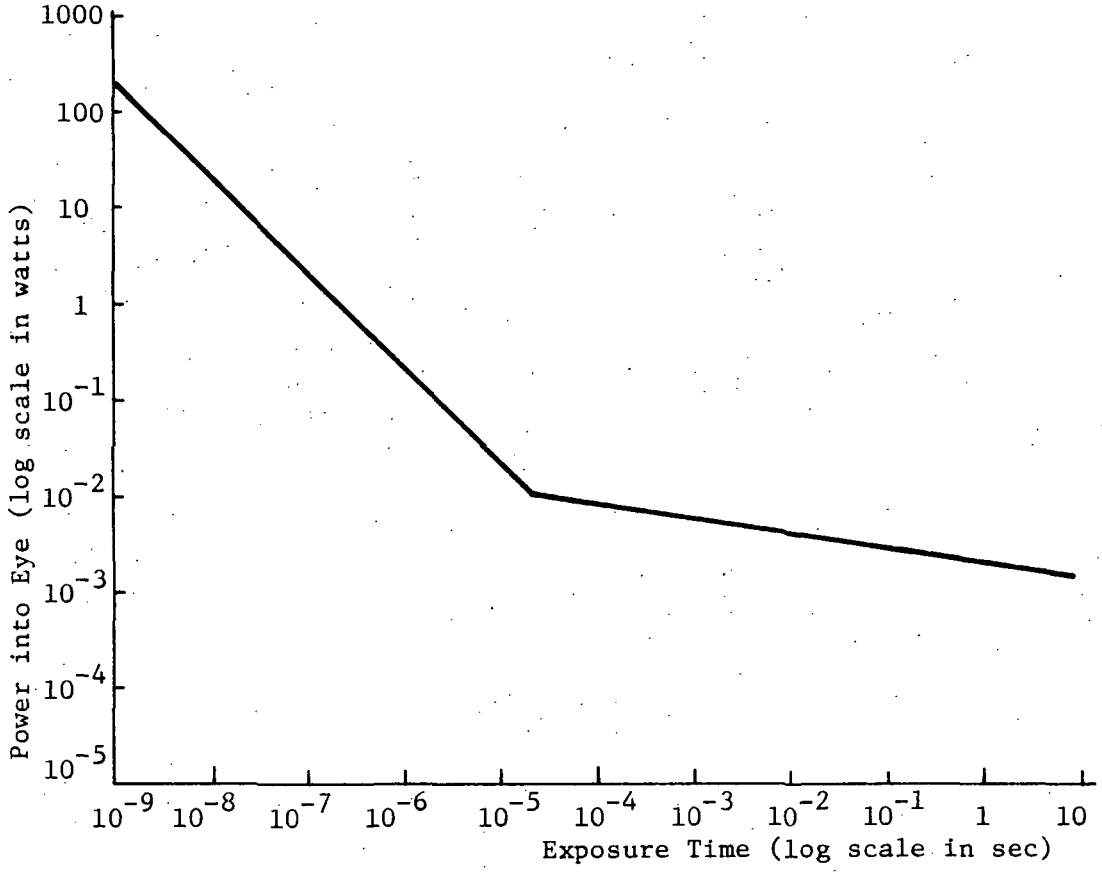

Fig. 4-16. Maximum radiation into eye for spectral range 0.4μ to 0.694μ per draft of American National Standards Institute, Standards on Laser Radiation (ref. 22).

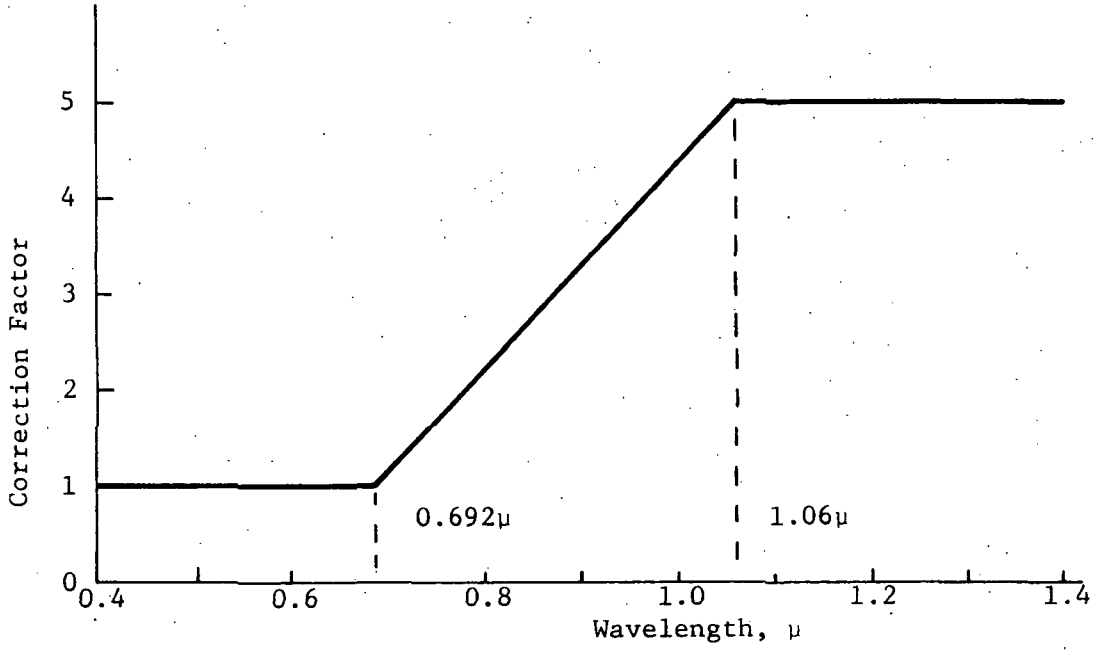

Fig. 4-17. Correction factor of allowable radiation into eye vs. wavelength per draft of American National Standards Institute, Standards on Laser Radiation (ref. 22).

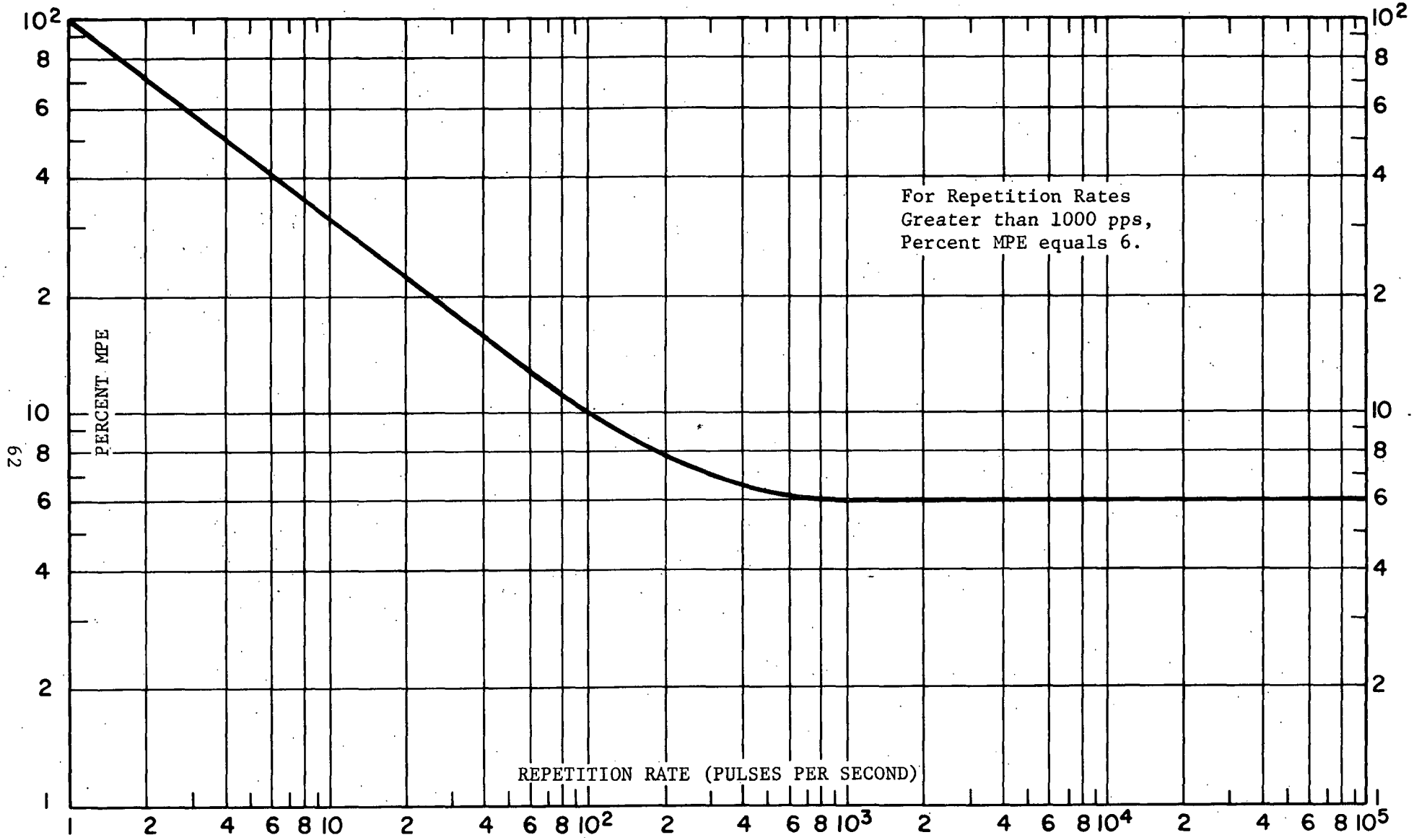

Fig. 4-18. Correction factor of allowable radiation into eye vs. pulse repetition rate per draft of American National Standards Institute, Standards on Laser Radiation (ref. 22).

$$D = \log_{10} \frac{1}{T}$$

where T is the relative intensity of light passed at the particular wavelength in question, and hence D is a measure of attenuation. Goggles exist as high pass, low pass, notch, and band pass filters. Consideration of these for radiation protection, however, must include the effects that they may have on the performance of the individual required to wear them. For example, a notch-type filter, designed to reject argon laser radiation (0.6328 μ wavelength) can cause color distortion, which would be objectionable to (and possibly impair the performance of) a pilot required to wear them.

The general concern about laser eye safety has created considerable interest in development of lasers that operate in spectral regions where the ocular media are relatively opaque to the incident radiation and hence where maximum permissible exposures are much greater. Erbium, which operates around a 1.6 μ wavelength, has been studied extensively for this reason (ref. 14), and more recently, holmium, which operates around a 2 μ wavelength, has been studied (ref. 24) because of the higher lasing efficiency it potentially provides. CO_2 lasers, operating at a 10.6 μ wavelength, are the only lasers at longer wavelengths that are readily commercially available (ref. 25). CO_2 laser radiation also has the advantage of experiencing less attenuation in the atmosphere and in fog.

4.2.4 Eye Safety Analysis

Three candidate laser systems have been considered for the laser tracker. Characteristics are as follows:

System No. 1

Laser type	NdYAG - pulsed
Wavelength	1.06 μm
Peak power	10^6 watt
PRF	100
Pulse width	20 nsec
Beamwidth	10 milliradians

System No. 2

Laser type	GaAs - pulsed
Wavelength	0.91 μm
Peak power	0.5 watt
Pulse rise time	20 nsec
Pulse width (estimated)	200 nsec
PRF	1000
Beamwidth	0.1 deg = 1.75 milliradians

System No. 3

Laser type	Nd:YAG - pulsed
Wavelength	1.06 μm
Peak power	6.7 Mw
PRF	40 pps
Pulse width	15 nsec
Beamwidth	2 milliradians

Using these characteristics, the laser radiation exposure levels are easily computed. It can be shown that the power per unit area in a uniformly illuminated beam is (when the radiating aperture is negligibly small compared to $R\theta$)

$$\frac{\text{power}}{\text{unit area}} = \frac{4P_t T_a}{\pi R^2 \theta_t^2}$$

where P_t = transmitter total power,
T_a = atmospheric transmittance,
R = laser to target range, and
θ_t = width of laser beam.

For completeness, eyesafe calculations for exposure levels must be based on both peak and average power levels. For the peak power case, one is mainly interested in the energy per pulse, thus

$$\frac{\text{energy}}{\text{unit area}} = \frac{4P_t T_a \tau}{\pi R^2 \theta_t^2}$$

where τ is the pulse width. For the average power case,

$$\frac{\text{Ave. power}}{\text{unit area}} = \frac{4P_t T_a \tau (PRF)}{\pi R^2 \theta_t^2}$$

where τ x PRF is the transmitter duty cycle.

Eyesafe ranges can now be computed by setting the energy and power to the MPE values e_{MPE} and P_{MPE} for the respective radiation wavelengths and solving for eyesafe range R_s. This results in

$$R_s = \left[\frac{4P_t T_a \tau}{\pi \theta_t^2 e_{MPE}}\right] 1/2$$

and

$$R_s = \left[\frac{4P_t T_a \tau (PRF)}{\pi \theta_t^2 P_{MPE}}\right] 1/2 \quad .$$

The value of e_{MPE} for the two laser types being considered is obtained directly from the tabulation of MPE values and the correction factor graph (Fig. 4-17)in Section 4.2.2, or (for the single pulse case):

$$\text{for Nd-YAG:} \quad e_{MPE} = 25 \times 10^{-7} \frac{\text{joule}}{\text{cm}^2}$$

$$\text{for GaAs:} \quad e_{MPE} = 17 \times 10^{-7} \frac{\text{joule}}{\text{cm}^2} \quad .$$

For determining values of P_{MPE}, an appropriate exposure time must be specified. The new ANSI standards proposed recognize that the human eye will instinctively avert acute discomfort resulting from such effects as heating from a laser beam such that exposure for more than 0.25 sec is all but impossible. Using 0.25 sec as the possible exposure time, the values determined for the P_{MPE} values are:

$$\text{for Nd-YAG:} \quad P_{MPE} = 1.29 \times 10^{-2} \text{ watts/cm}^2$$

$$\text{for GaAs:} \quad P_{MPE} = 8.75 \times 10^{-3} \text{ watts/cm}^2 \quad .$$

Substituting the above values of e_{MPE} and P_{MPE} and the laser system characteristics into the expressions for eyesafe range derived earlier results in the following simple expressions for eyesafe range (and including the correction factor for pulse repetition frequency (Fig. 4-18) in section 4.2.2):

For System No. 1 ,

Based on peak power: $R_s = 1.04\sqrt{P_t}$ ft

Based on ave. power: $R_s = 0.142\sqrt{P_t}$ ft

For System No. 2,

Based on peak power: $R_s = 29.59\sqrt{P_t}$ ft

Based on ave. power: $R_s = 13.10\sqrt{P_t}$ ft

For System No. 3,

Based on peak power: $R_s = 3.58\sqrt{P_t}$ ft

Based on ave. power: $R_s = 0.33\sqrt{P_t}$ ft

In deriving the above expressions, T_a was set to unity as a worst case. It is recalled also that P_t in these expressions represents peak power.

The minimum eyesafe range for each system is represented by the maximum of the two values computed by the two different methods. Thus, for System No. 1, the eyesafe range based on peak power is the appropriate value. For the nominal peak power of 10^6 watts specified for the system, the minimum eyesafe range is 1040 ft. In contrast, the appropriate value for System No. 2 is determined by the computation based on average power. For the 0.5 watt nominal peak power specified, the minimum eyesafe range is about 21 ft.

Candidate Laser Tracking System No. 3 contains a power programmer which adds 10 db attenuation whenever target range is less than 15,000 feet. This power programmer also adds another 40 db attenuation whenever target range is less than 5000 feet. These eyesafety attenuators have a positive feedback indication to verify proper attenuation. If verification is not met, the laser will automatically shut off. The power programmer contains an additional 60 db attenuation (for a total available attenuation of 110 db) which is used to normalize the received signal level. These attenuators, when inserted, further improve the eyesafety of the laser over that implied by the calculated R_s.

Thus for all three systems, the appropriate computation is based on peak power. Table 4-1 summarizes the minimum eyesafe range for the three systems considered.

Table 4-1. Summary of minimum eyesafe range (R_s).

System System	Nominal Peak Power	Minimum Eyesafe Range	Aircraft Range
#1	10^6 watts	1040 ft	All
#2	0.5 watts	21 ft	All
#3 without attenuators	6.7×10^6 watts	9250 ft	15,000 or more
#3 with attenuators (10 db attenuators)	67 watts	2920 ft	5,000 to 15,000
#3 with attenuators (50 db attenuators)		29 ft	less than 5000

Even though the above results will not likely apply directly to the actual laser tracker that will be procured for the runway facility, they do illustrate that the achievement of an eyesafe laser tracking capability is feasible. Based on these results, any of the systems considered would be adequate from the eyesafety viewpoint, since all anticipated laser-to-aircraft ranges are greater than the computed eyesafe range. With further consideration, the system designers may desire to increase the eyesafe range values to account for various effects such as possible hot spots in the beam, power fluctuations, and varying pulse widths. Whereas such considerations might appear to make System No. 1 marginal, additional safeguards such as power programming (as in System No. 3) and goggles are readily available.*

Minimum eyesafe range calculations of the above type serve to establish the power constraints under which the system is designed to operate. Since the ability to laser track within such constraints has been demonstrated, no difficulty in achieving eyesafe requirements is anticipated.

*Power programming is a specified requirement in the laser procurement specifications.

5.0 REFERENCES

1. Thompson, W. S.: An Analytical Investigation of Acquisition Techniques and System Integration Studies for a Radar Aircraft Guidance Research Facility, Phase II. NASA CR-111931, Research Triangle Institute, July 1971.

2. RCA: Final Report for Apollo Ships Instrumentation Radar Program (August 1964-October 1965). Contract NAS5-9720, Goddard Space Flight Center, April 1966.

3. NASA: Statement of Work for a Laser Tracking System. Statement of Work No. P-2546, Wallops Station, June 12, 1972.

4. NASA, Wallops Station: Statement of Work for Real-Time Data Interface and Display System and the Experimental Runway Facility Data System. Statement of Work No. P-2385, August 4, 1971.

5. Vega Precision Laboratories, Inc.: Vega Interrogation System, Models 642 and 643, Specifications. Vienna, VA, January 1972.

6. Wolf Research and Development Corporation: Final Technical Report for Kalman Program for Positioning Aircraft (KAPPA). Contract NAS6-1942, October 1971.

7. Ruedger, W. H.: ITOS-1/TIROS-M SRIR Signal Analysis and Evaluation Study. Final Report, NOAA Contract 0-35198, March 1972.

8. Niessen, F. R.: Control Theory Analysis of a Three-Axis VTOL Flight Director. M.S. Thesis, Pennsylvania State University Department of Aerospace Engineering, June 1971.

9. Meditch, J. S.: Stochastic Optimal Linear Estimation and Control. McGraw-Hill, 1969.

10. Ham, W. T., Jr., et al.: The Eye Problem in Laser Safety. Archives of Environmental Health, vol. 20, February 1970.

11. _____: Effects of Laser Radiation on the Mammalian Eye. Trans. of the New York Academy of Sciences, Series II, vol. 28, no. 4, February 1966, 517-526.

12. _____: Laser Radiation Protection. Proc. of the First International Congress of Radiation Protection, Rome, Italy, 5-10 September 1966.

13. Van Pelt, W. F., et al.: The Bioeffects of Light. Optical Spectra, vol. 5, no. 7, September 1971, 33-36.

14. Bresnick, G. H., et al.: Ocular Hazards of Q-Switched Erbium Laser.

15. Swope, C. H.: A Short Annotated Bibliography on Laser Eye Protection. 13th Annual Technical Symposium Proceedings, Society of Photo-Optical Instrumentation Engineers, August 1968, 421-425.

16. Farrer, D. N., et al.: The Effect of Threshold Macular Lesions and Subthreshold Macular Exposures on Visual Acuity in the Rhesus Monkey. Americal Industrial Hygiene Association Journal, vol. 31, March-April 1970, 198-205.

17. Vassiliadis, A.; Rosan, R. C.; and Zweng, H. C.: Research on Ocular Laser Thresholds. Final Report, Contract F41609-68-C-0041, Stanford Research Institute, August 1969.

18. Private discussions with William T. Ham, Jr., and James Walkenbach, Medical College of Virginia, Richmond, March 1972.

19. Pitts, et. al.: The Effects of Ultraviolet Radiation on the Eye. Report SAM-TR-69-10, USAF School of Aerospace Medicine, Brooks AFB, Texas, February 1969.

20. Anon.: Military Agrees on a Safety Standard and Commends it to ANSI Committee. Laser Focus, vol. 8, no. 2, February 1972, 10.

21. Anon.: Threshold Limit Values of Physical Agents Adopted by ACGIH for 1969. American Conference of Governmental Industrial Hygienists, 5-7.

22. Anon.: Safety Standard, ANSI Style: Here's What the Fuss is About. Laser Focus, vol. 8, no. 2, February 1972, p. 16.

23. Private discussions with M. Wolbarsht, Duke University Medical Center, Durham, NC, October 1972.

24. Anon.: Holmium Overshadowing Erbium as an "Eye-Safe" Laser Material. Laser Focus, vol. 8, no. 3, March 1972, 18.

25. Anon.: Laser Tables. 1972 Laser Focus Buyer's Guide, January 1972.